UNIVERSIDADE FEDERAL DO RIO GRANDE DO SUL
INSTITUTO DE CIÊNCIAS BÁSICAS DA SAÚDE
PROGRAMA DE PÓS-GRADUAÇÃO EM CIÊNCIAS BIOLÓGICAS:
BIOQUÍMICA

André Oliveira Borba

# Implementation of a fiber optics photometry system for analyses of activity in dopaminergic neurons of the Ventral Tegmental Area (VTA) of Wistar rats

## *Padronização da técnica de fotometria por fibra óptica para análise de atividade de neurônios dopaminérgicos da Área Tegmental Ventral (VTA) em ratos Wistar*

Porto Alegre
2019

André Oliveira Borba

# Implementation of a fiber optics photometry system for analyses of activity in dopaminergic neurons of the Ventral Tegmental Area (VTA) of Wistar rats

## *Padronização da técnica de fotometria por fibra óptica para análise de atividade de neurônios dopaminérgicos da Área Tegmental Ventral (VTA) em ratos Wistar*

Dissertation submitted to the Graduate Program in Biological Scienes: Biochemistry, in partial fulfillment of the requirements for the degree of Master of Sciences in Biochemistry.

*(Dissertação apresentada ao Programa de Pós-Graduação em Ciências Biológicas: Bioquímica do Instituto de Ciências Básicas da Saúde da Universidade Federal do Rio Grande do Sul como requisito parcial para a obtenção do título de mestre em Bioquímica.)*

**Advisor (Orientador):** Prof. Dr. Marcelo de Oliveira Dietrich (Universidade de Yale, New Haven, Estados Unidos)

**Co-Advisor (Co-orientador):** Prof. Dr. Diogo Onofre Gomes de Souza (Universidade Federal do Rio Grande do Sul, Porto Alegre, Brasil).

Porto Alegre

2019

CIP - Catalogação na Publicação

Borba, André
Implementation of a Fiber Optics Photometry System for Analyses of Activity in Dopaminergic Neurons of the Ventral Tegmental Area (VTA) of Wistar Rats / André Borba. -- 2019.
80 f.
Orientador: Marcelo Dietrich.

Coorientador: Diogo Souza.

Dissertação (Mestrado) -- Universidade Federal do Rio Grande do Sul, Instituto de Ciências Básicas da Saúde, Programa de Pós-Graduação em Ciências Biológicas: Bioquímica, Porto Alegre, BR-RS, 2019.

1. Neuroscience. 2. Fiber Photometry. 3. Dopamine. 4. Wildtype Wistar rats. I. Dietrich, Marcelo, orient. II. Souza, Diogo, coorient. III. Título.

Elaborada pelo Sistema de Geração Automática de Ficha Catalográfica da UFRGS com os dados fornecidos pelo(a) autor(a).

# PREAMBLE

## Presentation

This dissertation (written in English) is organized in three parts, in accordance with local rules of the *Graduate Program in Biological Sciences: Biochemistry* (UFRGS):

**Part I**: Introduction and Aims.

**Part II**: Materials and Methods and Results.

**Part III**: Discussion, Conclusion, Future Perspectives and References.

The experiments described here were performed in the Unidade de Experimentação Animal (UEA) of the Hospital de Clínicas de Porto Alegre (HCPA), in the Centro de Microscopia e Microanálise (CMM) of UFRGS and in the Laboratory 28 of the UFRGS Department of Biochemistry under the supervision of Prof. Dr. Marcelo de Oliveira Dietrich.

## Apresentação

Esta dissertação (escrita em inglês) está organizada em três partes, cada um sendo constituído dos seguintes itens:

**Parte I**: Introdução e Objetivos.

**Parte II**: Materiais e Métodos e Resultados.

**Parte III**: Discussão, Conclusão, Perspectivas e Referências.

Os experimentos descritos nesta dissertação foram realizados na Unidade de Experimentação Animal (UEA) do Hospital de Clínicas de Porto Alegre (HCPA), no Centro de Microscopia e Microanálise (CMM) da UFRGS e no Laboratório 28 do Departamento de Bioquímica da UFRGS, sob orientação do Prof. Dr. Marcelo de Oliveira Dietrich.

## ABSTRACT

This study depicts our efforts to implement the fiber photometry technology for monitoring of genetically-specified neuronal populations in adult and freely behaving wildtype Wistar rats. The brain region of choice was the dopaminergic ventral tegmental area of the brainstem. This region has been extensively correlated with reward and motivation. We injected adult Wistar rats with a 1:1 ratio of a commercial mix containing two viral vectors: one coding the Cre recombinase under the tyrosine hydroxylase promoter and other coding a floxed GCaMP6f gene. In the same surgery, a fiber optic cannula was placed right above the injection site and secured to the animal skull with screws and dental cement. After recovery from surgery, animals were submitted to behavioral paradigms designed to highlight dopaminergic functioning in relation to reward, reward prediction, frustration, and social interaction. Our results indicate that we have successfully implemented this technique in wildtype Wistar rats, but it also highlights the caution needed when utilizing bulk neuronal recording technology and interpreting its data.

## RESUMO

Este trabalho apresenta nossos esforços para padronizar a técnica de fotometria por fibra óptica para o monitoramento de populações neuronais geneticamente especificadas em ratos Wistar adultos *wildtype* enquanto os mesmos se comportam livremente. A região cerebral de escolha foi a centro dopaminérgico chamado de área tegmental ventral, no tronco encefálico. Esta região já foi extensivamente correlacionada com aspectos de recompensa e motivação. Uma mistura comercial de dois vetores virais numa proporção de 1:1 foi injetada nesta região do cérebro de ratos adultos: um que codifica a recombinase Cre sob a influência do promotor da tirosina hidroxilase e o outro que codifica o gene *floxed* para a GCaMP6f. Na mesma cirurgia, uma cânula de fibra óptica foi implantada imediatamente acima da região injetada e fixada ao crânio dos animais com o auxílio de parafusos e cimento dentário. Após recuperação pós-cirúrgica, os animais foram submetidos a protocolos comportamentais pensados para ressaltar a atividade dopaminérgica em paradigmas envolvendo recompensa, antecipação, frustração e socialização. Nossos resultados indicam que conseguimos atingir o objetivo de implementação e padronização da técnica de fotometria por fibra óptica em ratos Wistar *wildtype*, ao passo que também chamam a atenção para os cuidados necessários ao se utilizar técnicas de imageamento de atividade de populações neuronais e na interpretação dos dados obtidos por meio dessas técnicas.

# LIST OF ABREVIATIONS

AAV – adeno-associated virus

CNS – central nervous system

CS – conditioned stimulus

D1R – type 1 dopamine receptor

D2R – type 2 dopamine receptor

DA – dopamine

DLS – dorso-lateral stiratum

DMS – dorso-medial striatum

GECI – genetically encoded calcium indicator

GPCR – G-protein coupled receptor

MPFC – medial pre-frontal cortex

MSN – medium spiny neuron

NAc – nucleus accumbens

SN – substantia nigra

SNc – substantia nigra pars compacta

TH – tyrosine hydroxylase

US – unconditioned stimulus

VS – ventral striatum

VTA – ventral tegmental area

# Table of Contents

PART I ..... 8
1. INTRODUCTION ..... 9
1.1 GENETICALLY ENCODED CALCIUM INDICATORS (GECIs) ..... 11
1.2 Cre/*loxP* SYSTEM ..... 14
1.3 FIBER PHOTOMETRY ..... 16
1.4 DOPAMINE AND MOTIVATED BEHAVIORS ..... 18
2. AIMS ..... 25
2.1 GENERAL AIM ..... 25
PART II ..... 26
CHAPTER I – EXPERIMENTAL PROCEDURES ..... 27
1. ANIMALS ..... 27
2. STEREOTAXIC SURGERY FOR AAV INJECTION AND CANNULA PLACEMENT ..... 27
3. BEHAVIORAL PROCEDURE: SIMPLE REWARD PARADIGM ..... 29
4. BEHAVIORAL PROCEDURE: PRO-SOCIAL PARADIGM ..... 30
5. BEHAVIORAL PROCEDURE: CLASSICAL CONDITIONING AND FRUSTRATION PARADIGMS ..... 31
6. BEHAVIORAL PROCEDURE: SOCIAL ISOLATION AND FOOD DEPRIVATION PARADIGMS ..... 32
7. FIXATION OF TISSUE AND IMMUNOHISTOCHEMISTRY ..... 33
8. STATISTICAL ANALYSES AND DATA PLOTTING ..... 34
CHAPTER II – RESULTS ..... 35
INFECTION OF DOPAMINERGIC CELLS OF THE VTA BY A COMBINATION OF VIRAL VECTORS AND GENERAL CONSIDERATIONS ABOUT THE SURGERY ..... 36
DETECTION OF DOPAMINERGIC SIGNALING IN SIMPLE REWARD AND IN PAVLOVIAN CONDITIONING PARADIGMS POINT TO THE FUNCTIONAL DIVERSITY OF MESOLIMBIC DOPAMINERGIC CELLS ..... 41
DOPAMINERGIC VTA CELLS RESPOND TO SOCIAL INTERACTION ..... 55
PART III ..... 60
DISCUSSION ..... 61
FIBER PHOTOMETRY AS A TOOL FOR PROBING DOPAMINERGIC NEURONAL SUBPOPULATIONS IN WILDTYPE RATS ..... 61
CONCLUSION ..... 65
FUTURE PERSPECTIVES ..... 66
REFERENCES ..... 67

# PART I

This part contains the introduction and aims of this dissertation.

# 1. INTRODUCTION

As many other feats of engineering and technological advances, fiber optic photometry is a solution to a problem. Namely, how can one reliably record the activity of a specific neuronal population while not restraining naturally occurring behaviors?

For long, progress towards the understanding of the mammalian brain has followed two parallel paths: the anatomical and the functional. Breakthrough observations made by Golgi and Cajal allowed for a morphological comprehension of the neuron, whereas Hodgkin and Huxley's landmark studies on the giant squid axon allowed neuroscientists to uncover the ionic mechanisms that dictate neuronal functioning.

Electrophysiological methods, such as patch-clamp and single-unit voltage recordings, can be used to record and to alter neuronal activity in awake animals, but it is challenging to precisely determine the identity of the cells and circuits upon which the electrode is acting. So, although the study of the electrical properties of cells were, and continue to be, of paramount importance for enlightening neuronal function, electrode-based methods have their limitations.

On the other hand, morphological methods, such as microscopy, although being capable of providing information about determined and specified cell types and lineages, cannot, by their very own nature, provide information about the physiological properties of these neurons in real time. For instance, c-Fos staining for measuring activity does not allow investigation of the time relation of the neuronal activity and the behavior being analyzed (e.g. before and/or after the behavior occurs) in the same animal.

However, convergence of the molecular and systems branches of neuroscience has yielded unprecedented progress in understanding both the organizational and physiological properties of the nervous system. Much of these advances are due to the development of new genetic editing toolsets, as well as improvements in instrumentation. Of particular importance to the present work are the genetically encoded calcium indicators for reporting neuronal activity, the Cre/*loxP* recombination

technology that enables genetically-specific targeting of neurons and fiber photometry technology that allows for real time probing of deep brain structures in freely behaving animals.

## 1.1 GENETICALLY ENCODED CALCIUM INDICATORS (GECIs)

In order to better understand how the central nervous system (CNS) encodes and processes information at circuit and cellular levels, many efforts have been made towards the development of different optical indicators that can inform about neuronal activity.

In the nervous system, calcium ions ($Ca^{2+}$) have a high degree of functional versatility. Amongst other functions, this ion is responsible for triggering exocytosis of neurotransmitter-containing synaptic vesicles in the presynaptic terminal (NEHER; SAKABA, 2008); inducing activity-dependent synaptic plasticity in dendrites (NEVIAN; SAKMANN, 2006); regulating gene transcription in the nucleus (LYONS; WEST, 2011); and its influx and subsequent increase in intracellular concentration is tightly coupled with action potentials (AP) in neurons (BAKER; HODGKIN; RIDGWAY, 1971; SABATINI; OERTNER; SVOBODA, 2002). Consequentially, one approach taken to monitor neuronal activity is to measure fluctuations in intracellular $Ca^{2+}$ concentration ($[Ca^{2+}]_i$). This enables studies on neural ensemble dynamics and coding, dendritic processing, synaptic function, neural activity patterns and their correlation with behavioral expression (LUO; CALLAWAY; SVOBODA, 2018a).

In light of this, it is not surprising that calcium signalization and fluctuation have been an important focus of study in the neuroscience. The development of calcium imaging techniques involved two processes: the development and improvement of calcium indicators and the development and implementation of the appropriate instruments (GRIENBERGER; KONNERTH, 2012).

The development of protein-based genetically encoded activity indicators was one such process. These proteins are encoded in the DNA of a neuron, usually by means of genetic editing, and report a given neuronal property influenced by neural activity, such as $[Ca^{2+}]_i$ or transmembrane voltage, as changes in fluorescence (BROUSSARD; LIANG; TIAN, 2014). Optical reporters have been engineered for a myriad of cellular functions, such as vesicle release, changes in neurotransmitter

concentrations, transmembrane voltage, alterations in pH, and intracellular $Ca^{2+}$ dynamics (LIN; SCHNITZER, 2016).

Amongst the genetically encoded activity indicators, GECIs have seen major developments in sensitivity and reliability over the past decade. At rest, $[Ca^{2+}]_i$ is maintained at around 50 – 100 nM in neurons (BERRIDGE; LIPP; BOOTMAN, 2000). Neuronal activity, however, promotes the influx of $Ca^{2+}$ into the cytosol via multiple routes (intracellular storage, ionotropic receptors and voltage-dependent ionic channels), increasing the total $[Ca^{2+}]_i$ (GRIENBERGER; KONNERTH, 2012). Free calcium ions, although important in many signaling mechanisms, can be detrimental for the cell if kept at high cytoplasmic concentrations, because it can, for example, induce apoptosis. As such, naturally occurring proteins (e.g. SERCA and CaM) in neurons are responsible for chelating the free $Ca^{2+}$ before it can induce any cellular damage (CLAPHAM, 2007). Modern GECIs (Genetically Encoded Calcium Indicators) take advantage of this phenomenon. These are engineered proteins that emit fluorescence in the presence of free $Ca^{2+}$. They are based on fusions of fluorescent proteins and $Ca^{2+}$ binding proteins, such as calmodulin, that undergo conformational changes in response to $Ca^{2+}$ binding (CHEN et al., 2013).

The GCaMP family of proteins are the most widely used GECIs in neuroscience research (Figure 1). GCaMP proteins consist of a circularly permuted enhanced green fluorescent protein (cpEGFP) flanked on one side by calmodulin (CaM) and on the other side by the calmodulin-binding peptide M13. In the presence of $Ca^{2+}$, CaM-M13 interactions elicit conformational changes in the fluorophore environment that lead to an increase in the emitted fluorescence (AKERBOOM et al., 2012; NAKAI; OHKURA; IMOTO, 2001).

The GCaMP used for the current study, GCaMP6f, was developed by Chen and collaborators (CHEN et al., 2013). Their work reports the development of three variations of GCaMP6 with different kinetics and fluorescent properties: GCaMP6s (slow), GCaMP6m (medium) and GCaMP6f (fast). Whereas GCaMP6f has the least brightness in fluorescence upon $Ca^{2+}$ binding, it is also the indicator with the fastest kinetic properties of the three (CHEN et al., 2013).

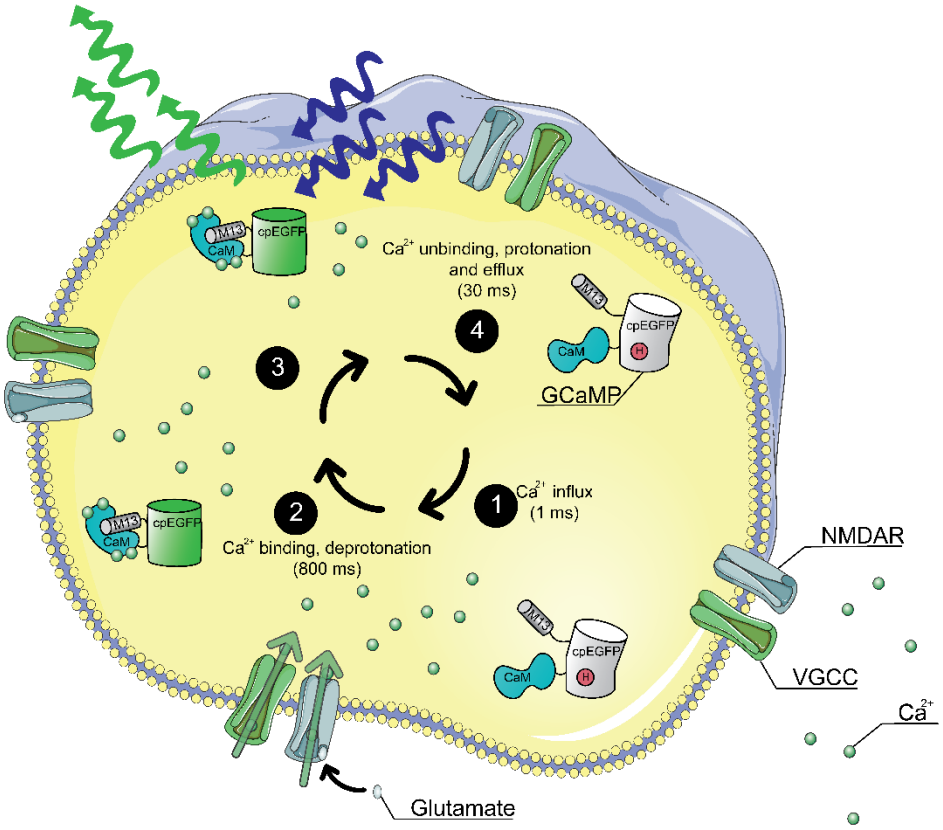


**FIGURE 1: Increased intracellular $Ca^{2+}$ concentration promotes conformational changes in GCaMP leading to increased fluorescence**

**(1)** Events following a glutamate release event (NMDAR activation) and single AP (Voltage-Gated Calcium Channels (VGCC) activation) are shown. **(2)** Calcium induced binding of CaM causes conformational changes in the cpEGFP, inducing loss of a proton from the chromophore and an absorbance shift. **(3)** GCaMP can report calcium transients with increased green emission (leftward green sinusoidal arrow) upon blue excitation (rightward blue sinusoidal arrow). **(4)** After $[Ca^{2+}]_I$ is normalized, the ions are released from the GCaMP and the protein assumes its original conformational properties. Image made by the author, adapted from LIN & SCHNITZER (2016).

## 1.2 Cre/*loxP* SYSTEM

The Cre/*loxP*-mediated recombination system is a versatile gene editing tool. The Cre recombinase is an enzyme from the tyrosine site-specific recombinase (T-SSR) family of proteins that promote site-specific recombination upon recognition of their respective, typically palindromic – that have the same base sequence regardless of reading direction (5'→3' or 3'→5') – recombinase target sites (RTs). Isolated from the P1 bacteriophage, this system is thus named because this enzyme causes recombination (Cre) in its binding site *locus of crossing over (x)* (*loxP*)(MCLELLAN; ROSENTHAL; PINTO, 2017). Since identified in 1981, biotechnological advances have created innumerous permutations of the Cre/*loxP* system that allowed for optimization of gene deletions, insertions and inversions with great spatial and temporal control, making it one of the most widely used tools for genetic editing (ANASTASSIADIS et al., 2010; GONG et al., 2007; ZHANG et al., 2012).

The mechanism by which this recombinase acts is contingent on two elements: the cell which the genome will be edited needs to (i) have a locus where a segment of DNA is flanked by two *loxP* sites, referred to as a "floxed" gene, and (ii) the same cell also needs to express the Cre enzyme. Recombination specificity is controlled by promoter and enhancer sequences that drive Cre expression in the cell or tissue type of interest (MCLELLAN; ROSENTHAL; PINTO, 2017; NAGY, 2000). There are different methods to achieve this goal. The most commonly used technique utilizes a combination of transgenic animal lineages that express Cre under a specific promoter and viral vector injection that delivers the floxed gene to the region of interest. Adeno-associated virus (AAV) vectors are the most commonly used for the delivery of a Cre-dependent floxed gene in a site-specific manner (MOROZOV, 2008; SONG; PALMITER, 2018). Once the enzyme is expressed and the floxed sequence is integrated into the cell DNA, there are three possible outcomes depending on the orientation of the *loxP* site (Figure 2): (i) excision/insertion of the floxed sequence, if the gene is flanked by two equally oriented *loxP* sites; (ii) inversion of the floxed sequence (and thereby its activation or inactivation, depending on its original orientation), if the gene if flanked by two conversely oriented *loxP* sites; or (iii) translocation/exchange of

the floxed sequence with another floxed sequence, if both are on linear but distinct DNA molecules (BRANDA; DYMECKI, 2004; ZHANG et al., 2012). This approach allows for genetic expression in a Cre-dependent manner in regionally and genetically specified cell lineage.

In the present study, we delivered a combination of viral vectors to our region of interest: a Cre viral vector that encodes the enzyme under a specific promoter (Tyrosine Hydroxylase), and a Cre-dependent viral vector encoding a floxed GCaMP6f gene. More details are provided in the Materials and Methods section.

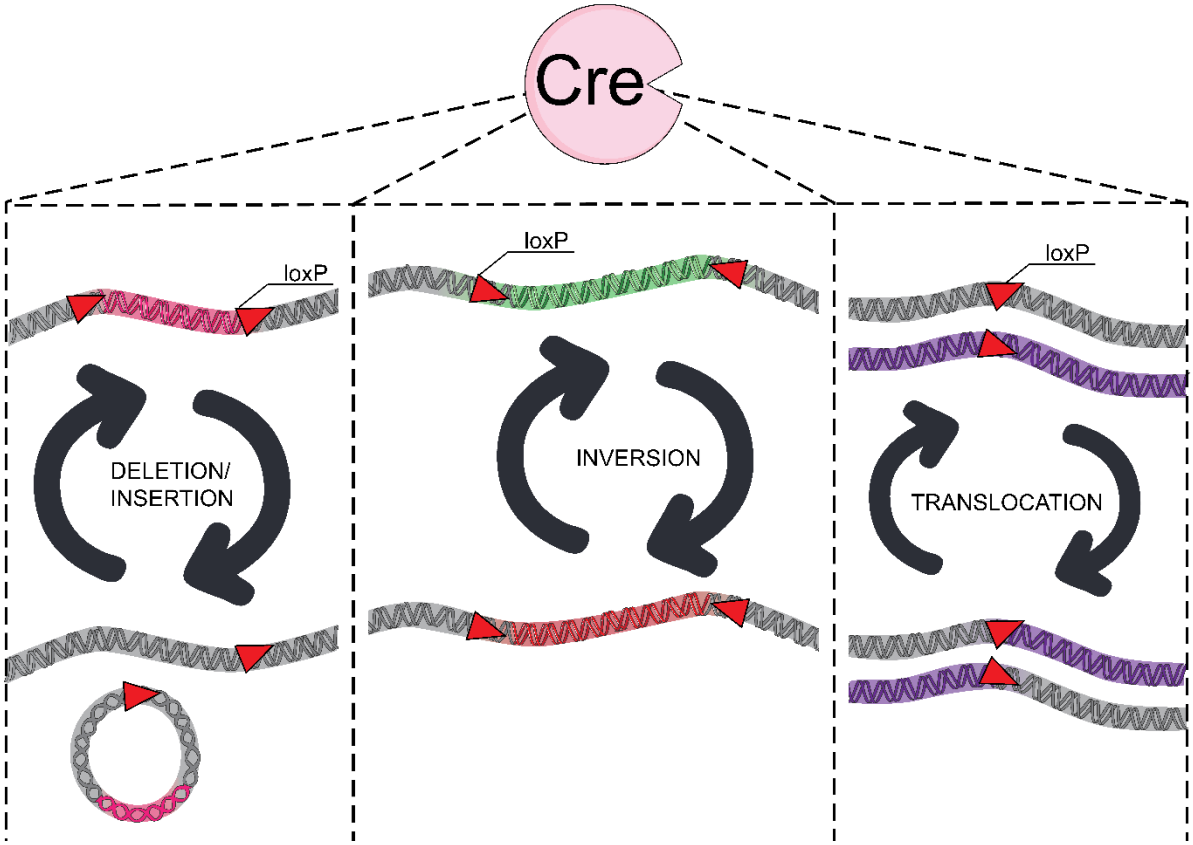


**FIGURE 2: DNA manipulations controlled by Cre abd *loxP* directions or locations**
The Cre enzyme has three modes of action: When one *loxP* is on a linear DNA while another is on a circular DNA, the circular DNA will integrate into the linear DNA at the target. Small circular DNA is easily lost in cells; hence, deletion occurs more easily than insertion. If the two *loxP*s are in the same direction on one DNA molecule, the DNA between them will be deleted (left row). If two *loxP*s are in opposite orientations, the DNA fragment between them will be inverted (middle row). The DNA molecule will exchange a segment if both *loxP*s lie on linear DNA molecules (right row). The red triangles are *loxP* sites, and indicate their direction. Image made by the author, adapted from ZHANG et al (2012).

## 1.3 FIBER PHOTOMETRY

A key approach for understanding neural cell dynamics and its correlated behavioral manifestations is the monitoring of neural activity in freely behaving animals (i.e. non-head fixed). Traditional methods of detecting such activity are limited by the difficulty of determining the genetic identity of the activated cells in real time while not limiting the animal's movement. This issue has been ameliorated by the optimization of genetically encoded indicators and tools for genetic editing, enabling the measurement of fluorescence changes in genetically specified neurons. This molecular approach has given rise to methods of cellular imaging with head mounted microscopy, allowing for $Ca^{2+}$ imaging of single neurons up to until a 500 μm depth (WARDEN; CARDIN; DEISSEROTH, 2014). However, these optic methods based on head mounted microscopy do not permit the recording of neuronal activity from deep brain structures bellow 500 μm and they are made more difficult by strong light scattering and absorption in neural tissue (LUO; CALLAWAY; SVOBODA, 2018b; SVOBODA; YASUDA, 2006).

This obstacle was circumvented when Cui and collaborators (CUI et al., 2013) developed an *in vivo* photometry system that could measure fluorescence of activated cells in deep brain structures based on a time-correlated single-photon counting (TCSPC)-based fiber optic system. In this study, AAV vectors containing Cre-Dependent floxed GCaMP5 were injected in the dorsal striatum (DS) of dopamine receptor type 1 (D1R)-Cre and dopamine receptor type 2 (D2R)-Cre transgenic mouse lineages, thus leading to the selective expression of GCaMP in medium spiny neurons (MSNs) that also expressed D1R or D2R. Subsequently, a multimodal optical fiber was implemented just above the site of injection, allowing for fluorescence measurement of the MSNs neurons while these mice were behaving freely (CUI et al., 2013, 2014) (Figure 3).

Since it has been first used, fiber optic photometry has been successfully applied in the physiological investigation of a myriad of neuronal subpopulations and their

relation to behavior. However, the majority of this extensive body of work has been done utilizing transgenic Cre mouse lineages. In the present work, our efforts were focused on implementing this technique on wildtype Wistar rats, which are of easier access in our Brazilian research context. Implementing this technique in wildtype Wistar rats allows for a better accessibility, as the necessity for transgenic Cre lineages is circumvented.

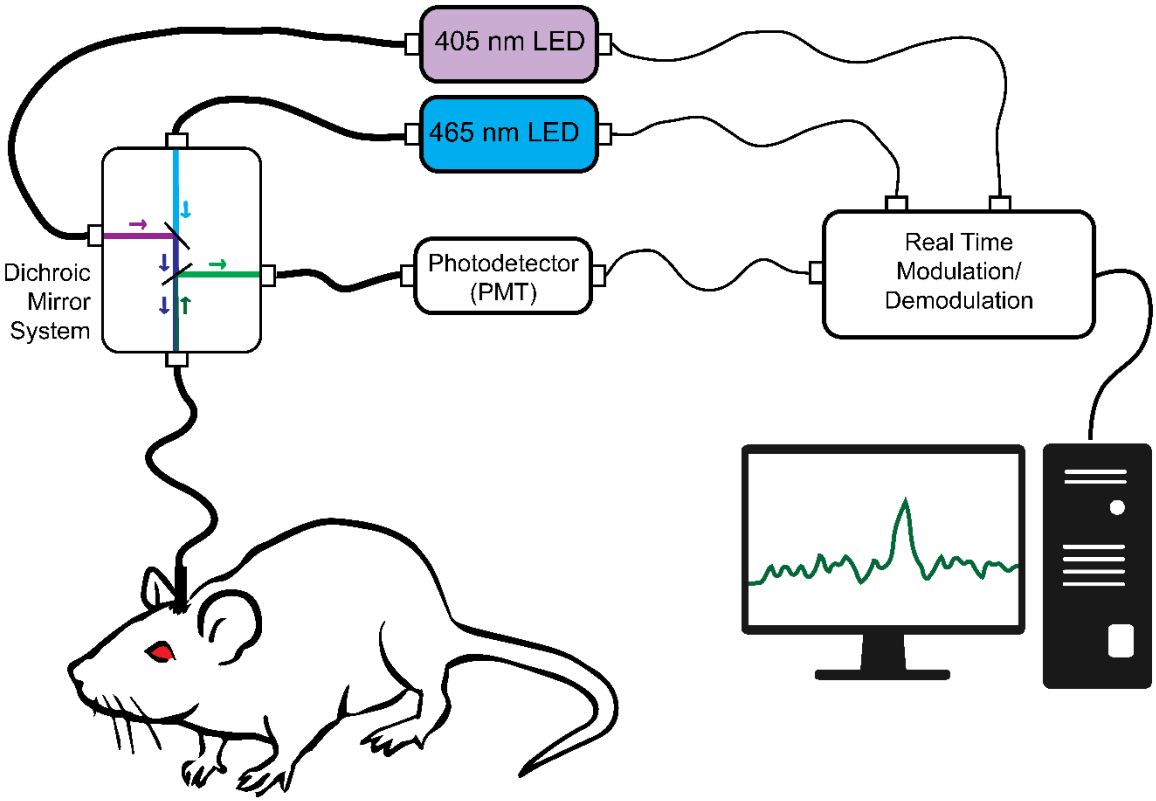


**FIGURE 3: Fiber Optic Photometry system setup**
405nm and 465nm LEDs are attached to a dichroic mirror box. The combination of these lights travels through a fiber optic patch cord into the fiber optic probe placed inside the animal's skull. Concomitantly, it carries back the green (488 nm) light emitted from GCaMP activity back into the dichroic mirror box, where it gets directed to a PMT for photo detection. The system is modulated in real-time through direct input from the computer. The wavelength separation is achieved through lock-in amplification and frequency decoupling. Image made by the author.

## 1.4 DOPAMINE AND MOTIVATED BEHAVIORS

Due to its relatively large size, well established electrophysiological and morphological characterization, as well as known reward-related behavioral correlations, the dopaminergic ventral tegmental area (VTA) of the midbrain was the region chosen to implement the fiber optic photometry system in the present work.

A brief introduction will be made on the physiology of dopamine (DA) and dopaminergic centers as well as their roles in modifying and expressing motivated behaviors.

### *1.4.1 DOPAMINE: PHYSIOLOGY, BIOCHEMISTRY AND ANATOMY*

In the 1930s, the brainstem was identified to have an important function in maintaining arousal throughout the whole brain (BREMER, 1936; KERKHOFS; LAVIE, 2000). In later studies it was uncovered that the midbrain, a region spamming from the rostral brainstem to the diencephalon, harbors many monamine (dopamine, norepinephrine, epinephrine, serotonin and histamine) and acetylcholine producing nuclei. Unlike other brain nuclei, these cholinergic and monoaminergic centers have a diffuse and widespread projection pattern throughout the whole CNS. Collectively, their function lies in regulating the autonomic nervous system, controlling the level of behavioral arousal, and influencing attention, mood, and memory (HUDSPETH, A.J.; SCHWARTZ, JAMES; SIEGELBAUM, STEVEN; KANDEL, ERIC; JESSELL, 2012).

Dopamine is a monoamine neurotransmitter from the catecholamine family, alongside norepinephrine and epinephrine. The first and rate-limiting enzyme in the catecholamine biosynthesis pathway is tyrosine hydroxylase (TH), an oxidase responsible for converting the amino acid tyrosine into L-dihydroxyphenylalanine (L-DOPA), which will be later converted into dopamine, epinephrine and norepinephrine; for this reason, TH is commonly used as a marker for dopaminergic and catecholaminergic neurons (HUDSPETH, A.J.; SCHWARTZ, JAMES; SIEGELBAUM, STEVEN; KANDEL, ERIC; JESSELL, 2012).

Dopamine is released from the presynaptic terminal into the synaptic cleft and exert its actions by binding to receptors present in the postsynaptic membrane. Dopamine receptors are in the large superfamily of G-protein coupled receptors (GPCRs), heterotrimeric metabotropic transmembrane proteins that are functionally classified based on its α subunit and the intracellular biochemical signaling cascade it generates upon activation (BEAULIEU; GAINETDINOV, 2011).

There are five subtypes of dopamine receptors: D1R, D2R, D3R, D4R and D5R; those can be classified into two families: D1-like receptors (D1R and D5R) and D2-like receptors (D2R, D3R and D4R). Receptors of the D1-like family, present exclusively in postsynaptic terminals, are $G\alpha_s$-coupled and thus stimulate adenylyl cyclase (AC), elevating $[cAMP]_i$. The D2-like family of receptors, on the other hand, are $G\alpha_i$-coupled and exert the opposite intracellular effect, being expressed in both pre- and postsynaptic terminals (SURMEIER; CARRILLO-REID; BARGAS, 2011). In terms of neural activity, dopamine main function is to modulate the excitability of its target neurons. Activation of D1R increases, whereas D2R activation decreases, glutamate receptor-mediated responses through modulation of ionic channels and receptors (ANDRÉ et al., 2010; BEAULIEU; ESPINOZA; GAINETDINOV, 2015; CEPEDA et al., 2008; CUMMINGS et al., 2008).

Major targets of midbrain dopamine input are the medium spiny neurons (MSNs) of the basal ganglia, large GABAergic inhibitory neurons involved in the CNS action selection mechanism. Histologically, MSNs present two phenotypes: D1-type or D2-type, which express either D1R or D2R, respectively (ANDRÉ et al., 2010; CEPEDA et al., 2008; GRILLNER; ROBERTSON, 2016)(GERFEN; SURMEIER, 2011; SURMEIER; CARRILLO-REID; BARGAS, 2011). Other important targets of DA inputs include the pre-frontal cortex (PFC) and its subdivisions, hypothalamus, and amygdala.

The cathecolaminergic nuclei are anatomically categorized in A groups (which produce epinephrine and dopamine) and C groups (which produce norepinephrine) that are sequentially numbered, from most caudal to most rostral. The dopaminergic nuclei in the midbrain comprise groups A8, A9 (substantia nigra), A10 (ventral tegmental area), A11-15 (hypothalamus) that have three major projections: nigrostriatal (or

mesostriatal), mesocorticolimbic and tuberoinfundibular pathways (HUDSPETH, A.J.; SCHWARTZ, JAMES; SIEGELBAUM, STEVEN; KANDEL, ERIC; JESSELL, 2012).

The mesocorticolimbic pathway arise from the VTA and send its projections to the olfactory bulb, amygdala, hippocampus, frontal cortex, and ventral striatum (VS), which includes the nucleus accumbens (NAc). Functionally, this pathway is more implicated in attention, reward, memory, learning, and other executive functions (MALENKA; NESTLER; HYMAN, 2009; NESTLER; HEYMAN; MALENKA, 2009). The nigrostriatal pathway, on the other hand, starts at the *Substantia Nigra pars compacta* (SNc) and projects to the dorsal-lateral and dorsal-medial striatum (DLS and DMS) (caudate and putamen), being more involved in the control of voluntary movement (MISHRA; SINGH; SHUKLA, 2018), although correlations of DA input to the DLS and DMS with reward and motivation have been established (GUNAYDIN et al., 2014; PALMITER, 2008; SZCZYPKA et al., 2001; ZHOU; PALMITER, 1995).

While DA projections from the SNc are more implicated in motor loops among cortical and subcortical structures, DA projections from the VTA comprise the non-motor loops. Architecturally, these loops follow similar input-output structure: cortex > striatum > globus pallidus > thalamus > cortex. However, the substructures which they entail are different. Whereas the motor loops (body movement loop and oculomotor loop) involve cortical motor areas, the non-motor loops (prefrontal loop and limbic loop) involve cortical areas correlated with cognition and emotion (such as the dorsolateral prefrontal cortex (DLPFC) and the anterior cingulate cortex (ACC)). Both the striatal substructures and the origin of their input also differ: while cortical areas responsible for movement project to the DLS and DMS (which receive DA input from the SNc), the areas involved with executive functions project to more ventral and anterior areas of the striatum, such as the NAc (which receive DA input from the VTA). The structural similarities among these loops suggest that the non-motor loops might play a role in regulation of behavior similar to the one played by the motor loops in control of movement (NICOLA, 2007; PURVES et al., 2012).

### *1.4.2 DOPAMINE: MOTIVATION AND GOAL-DIRECTED BEHAVIORS*

The concept of motivation is an elusive one. The matter has been tackled by different approaches in different fields, and a variety of postulates have been made in order to address the question of “what is motivation?”

Examples of behaviors that are not considered motivated can be found in the works of the ethologist Nikolaas Tinbergen. In his work, Tinbergen identified the fixed action pattern, a behavioral expression which always presents similar vigor, has a defined action sequence, is triggered by a specific environmental stimuli (releaser), and which manifestation is independent of learning (although it can affected by learning)(TINBERGEN, 1965). In this sense, a fixed action pattern resembles more a reflex movement (or a sequence of reflex movements) than the deliberate and motivated actions seen in motivated behaviors, such as foraging for food in food-seeking behaviors.

On the other hand, many attempts have been done in theoretically defining motivation and “drive”. In early uses of these words, motivations and drives only seemed to differ from reflexes in complexity of action, but with no underlying qualitative distinction. In his 1987 publication, Wise proposed that motivation should be understood as the result of motivational states. In this view, motivational states do not elicit a behavior *per se*, but rather provide modulatory information (of hormonal and/or neuronal origin) that bias the organism toward or away from a given situation, condition or outcome (WISE, 1987). Motivation can thus be understood as the biological process by which an animal becomes energized to engage in goal-directed behaviors and that is influenced by both external (sensory cues) and internal (physiological, affective, and cognitive) states (PALMITER, 2008), enabling organisms to regulate the proximity, probability and availability of stimuli (SALAMONE et al., 2015a). A goal-directed behavior, in its turn, is any behavior that seeks to accomplish a goal and can be divided in two distinct phases: approach behavior and consummatory behavior. The former describes the behavioral process of responding to sensory cues that will increase the likelihood of accomplishing such goal (e.g. foraging for food), whereas the latter refers

to what actions are taken after this goal is reached (e.g. eating) (SALAMONE et al., 2015b; SALAMONE; CORREA, 2012).

Interestingly, when providing examples of what could be responsible for these modulatory properties of motivational states, Wise himself cites dopamine as a possible candidate (WISE, 1987). Today it is broadly accepted that dopamine plays a fundamental role in movement and motivation (HOWE; DOMBECK, 2016; PALMITER, 2008; SALAMONE et al., 2015c; SALAMONE; CORREA, 2012; WISE, 2004), precisely by increasing or decreasing the threshold of activation of MSNs in the basal ganglia, the major targets of dopaminergic input from two major dopaminergic midbrain nuclei: the ventral tegmental area (VTA) and the *substantia nigra* (SN) (IKEMOTO; YANG; TAN, 2015; OGAWA; WATABE-UCHIDA, 2017; WATABE-UCHIDA et al., 2012).

Dopamine has been deemed the “pleasure” neurotransmitter due to findings in addiction studies that reported a peak of dopamine upon the use of recreational drugs and attributed this finding to the habit formation seen in drug users (FIBIGER, 1978). Accordingly, an extensive body of work grounded on single-unit recordings on awake and behaving non-human primates has shown DA-VTA neurons to have characteristic phasic responses to rewards and reward-predicting cues while being inhibited by aversive events (FIORILLO, 2013; STAUFFER et al., 2016; UNGLESS; MAGILL; BOLAM, 2004).

However, this approach to dopamine function fails to explain other findings relating the neurotransmitter with motivation, reward prediction, reinforcement learning, among other behavioral aspects (WISE, 2004). Studies using classical or Pavlovian conditioning paradigms have identified VTA-DA neurons that change their response over time: when pairing a rewarding unconditioned stimulus (US), such as food, to a conditioned stimulus (CS), a subpopulation of DA neurons will initially respond to both stimuli but will eventually only respond to the CS. If the reward, at some point, becomes bigger than expected these neurons become responsive again. This observation links DA function directly to the ability of outcome prediction through experience and learning (BROMBERG-MARTIN; MATSUMOTO; HIKOSAKA, 2010a; STEINBERG et al., 2013). Likewise, studies that take an instrumental or Skinner conditioning approach have

linked DA transmission with incentive salience (the process through which a stimulus is conferred with motivational properties that make it more attractive), exertion of effort, decision making, effort-outcome cost balance (how much effort should be exerted into a given task based on its expected reward), risk assessment and probability-based outcome prediction (BEELER; FRAZIER; ZHUANG, 2012; BEIERHOLM et al., 2013; HOWE et al., 2013; SATOH et al., 2003; SCHULTZ, 2010; WESTBROOK; FRANK, 2018).

More recent hypothesis on dopamine physiology suggest that anatomically and functionally distinct midbrain dopaminergic neuron subtypes may encode different signals and participate in largely separate circuits (BROMBERG-MARTIN; MATSUMOTO; HIKOSAKA, 2010a; GUNAYDIN et al., 2014; LAMMEL; LIM; MALENKA, 2014; LERNER et al., 2015; LIU et al., 2018; MENEGAS et al., 2018; MORALES; MARGOLIS, 2017; PALMITER, 2008; SALAMONE; CORREA, 2012; WATABE-UCHIDA; ESHEL; UCHIDA, 2017; WISE, 2004). This is supported by findings that reveal the diversity of neuronal subtypes in the dopaminergic nuclei in the midbrain, be it regarding expression profiles (MARGOLIS et al., 2010; POULIN et al., 2014), connectivity (BEIER et al., 2015; WATABE-UCHIDA et al., 2012), or physiology (BROMBERG-MARTIN; MATSUMOTO; HIKOSAKA, 2010a; DE JONG et al., 2019; GORE; SODEN; ZWEIFEL, 2014). Taken together, studies on connectivity and functional properties of mesolimbic DA neurons point to the existence of heterogeneous neuronal subpopulations that encode for different behavioral and motivational properties, such as reward, avoidance, prediction-error, incentive salience, modulation of effort, amongst other behavioral phenomena (Figure 4).

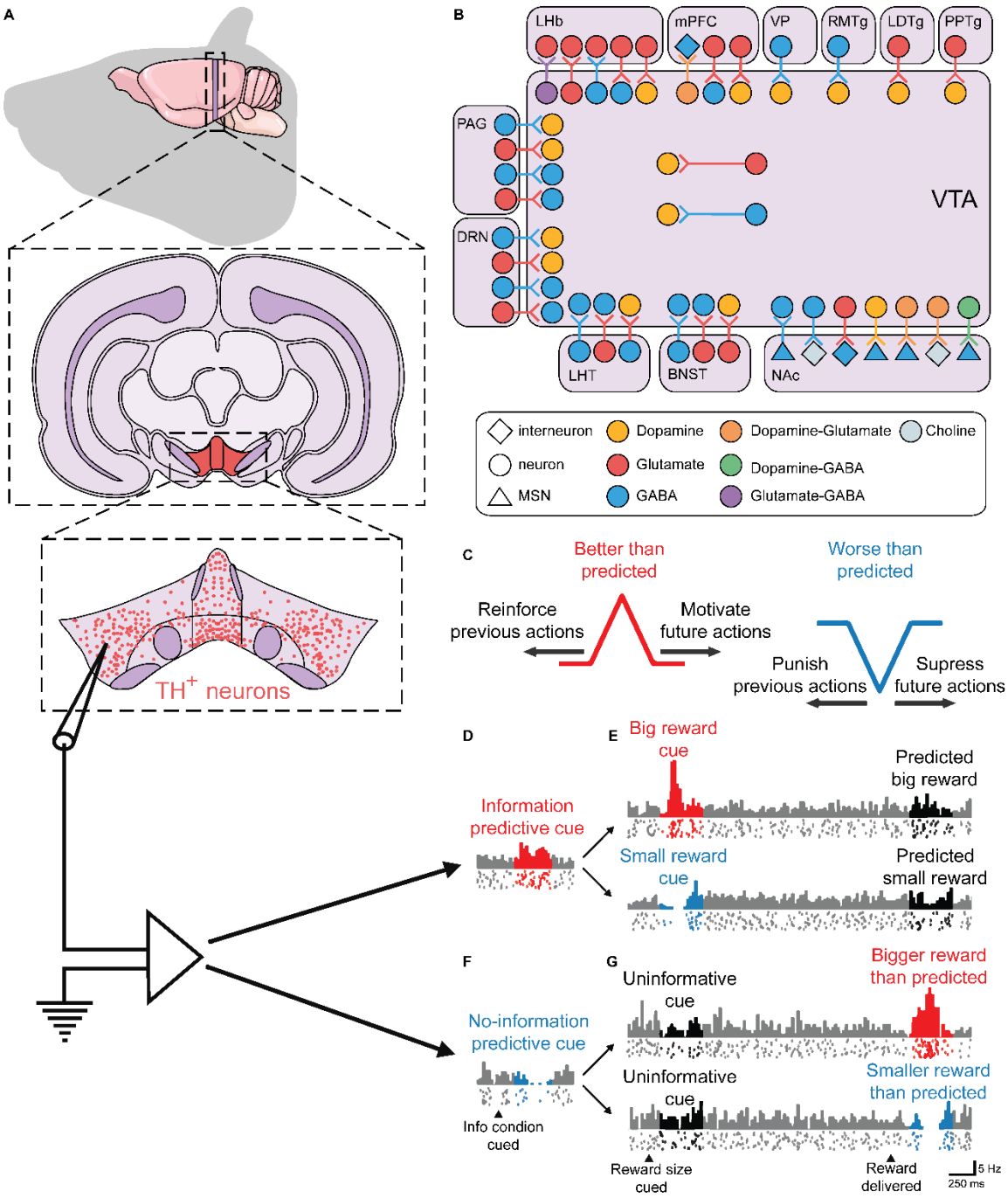


**FIGURE 4: DA VTA cells are functionally diverse and widely connected**
**(A)** Illustration detailing the location of the VTA. **(B)** The schematics summarize the synaptic connections that have been detected either anatomically (using electron microscopy) or functionally (using optogenetics in conjunction with *ex vivo* electrophysiology). VTA dopamine neurons receive glutamatergic inputs from the medial prefrontal cortex (mPFC), pedunculopontine tegmentum (PPTg), laterodorsal tegmentum nucleus (LTDg), lateral habenula (LHb), periaqueductal grey (PAG), bed nucleus of the stria terminalis (BNST) and dorsal raphe nucleus (DRN). VTA dopamine neurons receive GABA inputs from the rostromedial mesopontine tegmental nucleus (RMTg; also known as the tail of the VTA), PAG, DRN, lateral hypothalamus (LHT) and ventral pallidum (VP). There are also local glutamate and GABA synapses onto VTA dopamine neurons arising from neurons within the VTA.
**(continues next page)**

# 2. AIMS

## 2.1 GENERAL AIM

To implement a fiber photometry system to record the neuronal activity dynamics of dopaminergic mesolimbic VTA neurons in motivation-related behaviors in freely moving wildtype Wistar rats.

**FIGURE 4 (continues from the previous page): DA VTA cells are functionally diverse and widely connected**
VTA GABA neurons receive glutamatergic inputs from the LHb and mPFC and GABAergic inputs from the nucleus accumbens (NAc) medium spiny neurons (MSNs) expressing D1R. VTA GABA neurons receive both glutamatergic and GABAergic innervation from the PAG, DRN, LHT and BNST. Most BNST projections establishing synapses in the VTA are from GABA neurons that preferentially synapse on the VTA GABA neurons. VTA "GABA-only" neurons target cholinergic interneurons of the NAc and glutamatergic neurons of the LHb. VTA "glutamate-only" neurons target glutamate neurons of the LHb and nAcc PV-expressing neurons, whereas VTA combinatorial glutamate-GABA neurons target glutamate neurons of the LHb. VTA "dopamine-only" neurons establish symmetric synapses on MSNs, NAc cholinergic interneurons, and mPFC PV-expressing GABA-releasing interneurons; The combinatorial dopamine-GABA neurons target NAc MSNs. **(C)** Conventional theories of DA reward signals. DA neurons encode a reward prediction error signal, responding with phasic excitation when a situation's reward value becomes better than predicted (red) and phasic inhibition when the value becomes worse than predicted (blue). These signals could be used for learning, to reinforce or punish previous actions (backward arrows), or for immediate control of behavior, to promote or suppress reward-seeking actions (forward arrows). **(D-G)** An example DA neuron with conventional coding of reward prediction errors as well as coding of the subjective preference for predictive information. Each plot shows the neuron's mean firing rate (histogram, top) and its spikes on 20 individual trials (bottom rasters) during each condition of the task. Data are from Bromberg-Martin and Hikosaka (2009). **(D)** This DA neuron was excited by a cue indicating that an informative cue would appear to tell the size of a future reward. **(E)** DA excitation by big reward cue (red), inhibition by a small reward cue (blue), and no response to predictable reward outcomes (black). **(F)** This DA neuron was inhibited by a cue indicating that an uninformative cue would appear that would leave the reward size unpredictable (blue). **(G)** DA lack of response to uninformative cues (black), excitation by an unexpectedly big reward (red), and inhibition by an unexpectedly small reward (blue).
**(A-B)** Adapted from Morales and Margolis (2017). **(C-G)** Adapted from Bromberg-Martin, Matsumoto and Hikosaka (2010). Image made by the author.

# PART II

Here, the Methods and Materials and Results, as well as its interpretations, of this dissertation will be described.

# CHAPTER I – EXPERIMENTAL PROCEDURES

## 1. ANIMALS

In total, 31 adult Wistar rats, 24 males and 7 females, were used in the experimental procedures described here. All animals were provided by CREAL-UFRGS (Centro de Reprodução e Experimentação de Animais de Laboratório – Universidade Federal do Rio Grande do Sul) and housed in the UEA-HCPA (Unidade de Experimentação Animal – Hospital de Clínicas de Porto Alegre) animal facility. All behavioral and surgical procedures were performed in UEA-HCPA.

All animals were kept in temperature- and humidity-controlled rooms, in a 12/12 light/dark cycle, with lights on from 7:00 AM to 7:00 PM. Food and water were provided *ad libitum*. Before surgical procedures, all animals were kept in cages of either 2 or 3 cagemates. After surgical procedure, the animals were housed individually (unless otherwise stated in the text) in order to minimize risk of helmet detachment. All procedures were approved by the CEUA-HCPA (Comitê de Ética em Uso de Animais).

## 2. STEREOTAXIC SURGERY FOR AAV INJECTION AND CANNULA PLACEMENT

Rats were given a pre-surgical analgesia of 20 mg/Kg of tramadol i.p., and anesthetized with isoflurane 5%. The hair on top of their heads was shaved, and they were then placed on the stereotaxic apparatus (Kopf Instruments). The isufluorane flow was reduced to 1–2%. Oxygen flow rate was kept at 0.5 l/min. The surgical area was disinfected using chlorhexidine 2% and further local anesthesia was made by injection of s.c. bupivacaine (20 mg/Kg). The skin at the surface of the head was removed with a pair of sterile scissors, exposing the surface of the skull. A hydrogen peroxide solution was applied and rubbed on the skull surface with a cotton applicator in order to remove residual soft tissue and to better visualize the bregma. The coordinates for the left VTA were consulted (PAXINOS; WATSON, 1998) and a 1 mm hole was drilled at $x_{bregma}$ + 8 mm and $y_{bregma}$ - 5.3 mm. Additional two burr holes were drilled on the left and right parietal lobes of the skull for anchoring screws. A Hamilton Neuros Syringe (Hamilton)

containing 250 nl of each AAV viral vector (AAV1.CAG-Flex-GCaMP6f at titer $1.13x10^{13}$ and AAV9.rTH.PI.Cre.SV40 at titer $6.98x10^{13}$) was attached to the vertical arm of the stereotaxic apparatus and placed immediately above the hole drilled at the aforementioned coordinates. The syringe was lowered until it touched the brain surface and the *z* axis coordinate was recorded. The needle was then lowered 8.1 mm ($z_{bregma}$ - 8 mm) and the viral mix (0.5 µl total) was slowly injected over a period of 10 minutes (0.1 µl/min), after which the needle was left in place for 5-10 minutes before being removed. An 8 mm fiber optic cannula (Doric Lenses) was placed in the hole and lowered with the aid of a special stereotaxic arm attachment (THOR Labs | CX7 Adapter Arm Ø7.9 mm and XCF Cannula Holder for Ø2.5 mm Ferrules) until all the optic fiber portion of the probe was entirely inside the skull. Dental cement was applied on the skull exposed area, covering the two small screws as well. The rats were then placed in a

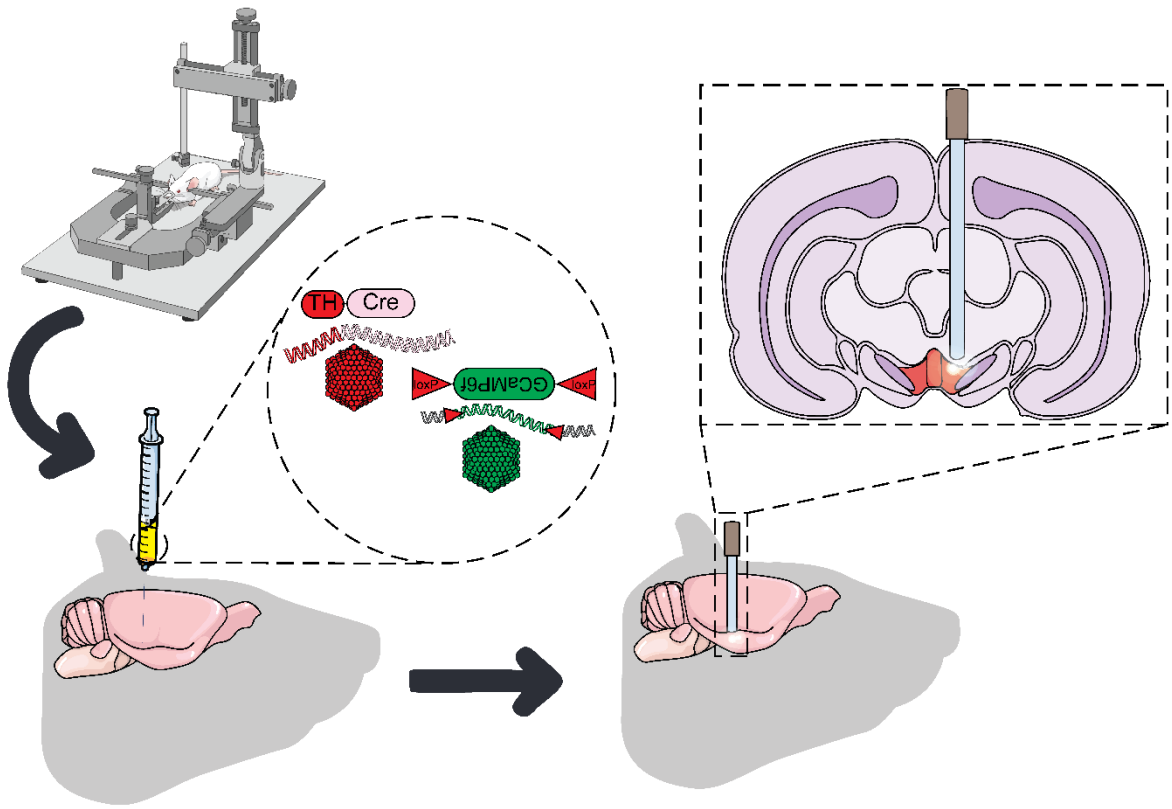


**FIGURE 5: Scheme of stereotaxic surgery for AAV injection and probe placement**
The anesthetized animal is placed on the stereotaxic apparatus and the bregma coordinates are taken. After the desired coordinates are found, the skull is drilled and the AAV mix is injected at the desired depth. Afterwards, the fiber optic cannula is placed immediately above the injection site. Illustration made by the author.

separate cage on a warm incubator (FANEM | Model: C 186 TS) for recovery at 30ºC and 40-60% humidity. For the 3 days after surgery, a 12 hours regimen of 20 mg/kg tramadol i.p. analgesic protocol was followed.

Surgical procedures are summarized in Figure 5(Figure 5).

### 3. BEHAVIORAL PROCEDURE: SIMPLE REWARD PARADIGM

Dopamine activity upon reward presentation is well documented (BROMBERG-MARTIN; MATSUMOTO; HIKOSAKA, 2010b). So, for our first tests, we aimed to standardize fiber photometry to measure calcium transient activity (as changes in *ΔF/F)* from VTA-DA in response to reward presentation. The apparatus where recordings were performed consists of an open field (54 cm x 43 cm x 59 cm). Rats had their probe attached to the fiber photometry system and were then placed in the open field. After 10 minutes of baseline fiber photometry recordings, rats were given a 30% sucrose solution at the 720 s mark. The trial was over after 900 s.

A caveat of using 30% sucrose was that we could not distinguish licking bouts from when the animal was simply with the head on top of the sucrose dish. To circumvent that, we started presenting the animals with 5 sunflower seeds, a reward for which they have a clear taste, was widely available at the animal facility, and we could capture the timestamps for when the animal grabbed and ate the seeds. The baseline photometry recording lasted 300 s. Rats received the sunflower seeds twice during the behavioral trial: 5 seeds at 420 s and 5 seeds at 540 s. The trial was over after 600 s.

The trial was captured, scored and analyzed using Any-MAZE 5.3 (Stoelting). The fiber photometry system consisted of two different sets of LEDs: 405 nm LED sinusoidally modulated at 531 Hz and a 465 nm LED sinusoidally modulated at 211 Hz. Both light streams were merged into an optical fiber patch using a minicube (Doric Systems). The fiber optic patch was connected to the cannula on the rat. Fluorescence emitted by GCaMP6f in response to light excitation was collected with the same patch cord and focused into a photomultiplier and photodetector (Doric Systems). The signal collected at the photodetector was redirected to a digital fiber photometry processor

(Doric Systems). Signal was processed and pre-analyzed using the Doric Neuroscience Studio software (Doric Systems). The data was exported to MATLAB 2018b (MathWorks) for post-processing. First, the isosbestic channel (405 nm excitation, denoted as $F_0$) was fitted to the calcium-dependent channel (465 nm excitation, denoted as $F$) using first order polynomial fitting. The normalized calcium fluorescence activity ($\Delta F/F$) was calculated as: $\Delta F/F = (F - F_0)/F_0$. Before every photometry recorded trial depicted in this dissertation, the light output was measured (μW) as a function of the voltage (V) applied to the LEDs used for the trials with the aid of a powermeter (THOR labs | Model: PM100D | Serial Number: P0016712). The most commonly used voltage for setting the LED lights were 0.4 to 0.7V, which corresponds to an average light output of 94.81μW (+/- 15.39μW) for the 405nm LED and 32.53μW (+/- 3.62μW) for the 465nm LED.

## 4. BEHAVIORAL PROCEDURE: PRO-SOCIAL PARADIGM

Rodents are highly social animals and heightened dopaminergic activity upon social interaction has been recorded in these animals (GUNAYDIN et al., 2014). With that in mind, we set out to investigate whether we could detect dopaminergic activity in a pro-social paradigm we standardized in our lab. The apparatus used for these behavioral trials consisted of a three-chamber apparatus, named chambers A (observer chamber) (44 cm, x 34 cm x 40 cm), B (44 cm x 34 cm x 40 cm) and C (demonstrator chambers) (44 cm x 34 cm x 40 cm) (Figure 6). In this paradigm, an observer rat is put in chamber C for 60 s for signal stabilization. At the 60 s mark, the demonstrator rat was inserted in chamber B and the observer rat was moved to chamber A and 5 sunflower seeds were added into chamber C. In chamber A, the observer rat could climb a platform (10 cm x 23 cm) that would open a sliding door (10 cm x 10 cm) located between chambers B and C, allowing the demonstrator rat to move to chamber C and have access to a reward (sunflower seeds). The trial was completed 120 s after the observer opened the door. If the observer did not climb the platform in order to open the sliding door, the test would be over at the 420 s mark. As control trials, we presented the animals with a simple reward of sunflower seeds (as done in the previous experiments) in chamber C

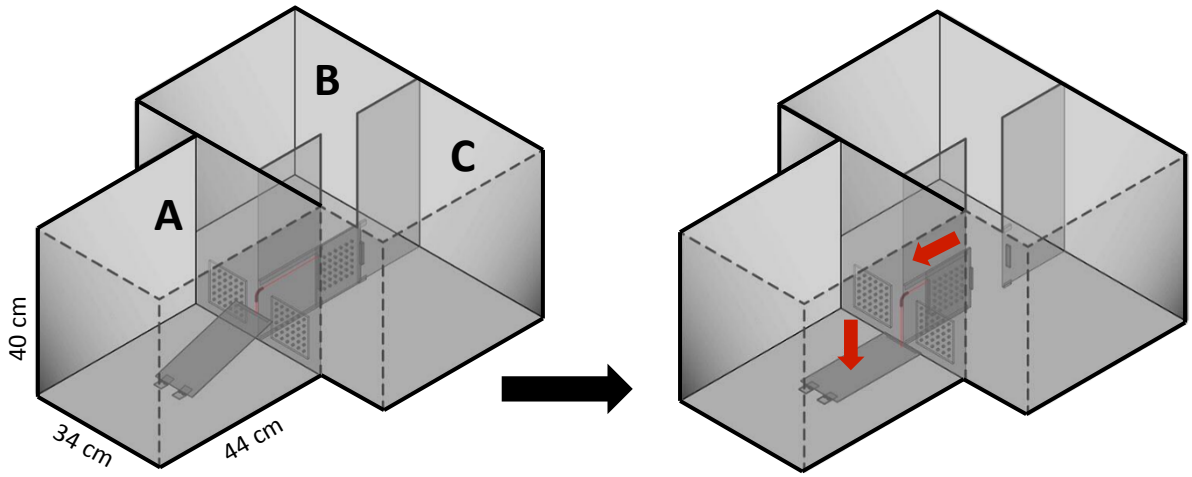


**FIGURE 6: Schematic illustration of the pro-social apparatus**
The apparatus consists of three equally sized chambers (40 cm x 34 cm x 44 cm): A (observer), B and C (demonstrator). In chamber A, the observer rat can climb a platform. This platform is connected to the sliding door between chambers B and C through a thin metal wire. Thus, when the observer animal climbs the platform, the sliding door opens. This allows the demonstrator rat, originally placed in chamber B, to have free access to chamber C. The platform dimensions are 10 cm x 23 cm; the sliding door dimensions are 10 cm x 10 cm. Image made by the author.

at the 30 s mark and the trial lasted for 120 s; and performed an empty control trial in which no demonstrator was added to the apparatus, following the same time stamps of the pro-social trials. We performed the surgery for viral vector injection and cannula placement in 10 animals for this set of experiments, all of which had been previously trained in the task (animals #16 to #25). The experiment regimen consisted of 17 trials, one trial a day. Since only animals #23 and #24 survived through the whole experiment regimen as a pair, only the data from these animals will be considered. All animals were being housed individually for the duration of the experiments. Trials in which photometry data was acquired are highlighted in figure 12. Photometry and behavioral data were recorded and analyzed as previously.

## 5. BEHAVIORAL PROCEDURE: CLASSICAL CONDITIONING AND FRUSTRATION PARADIGMS

Dopaminergic VTA neurons have been shown to alter their response after conditioning, as well as responding differently upon frustration (DE JONG et al., 2019;

MOHEBI et al., 2019). For this reason, we tested if we could detect a change in the captured signal profile throughout sequential conditioning trials and how a frustration paradigm could interfere in such signal. The apparatus used for these behavioral trials was the same used for the pro-social behavioral procedure. Only chambers B and C were used in this set of experiments. Rats did not have access to chamber A. Animals were placed in chamber B for 120 s, at which point a sound cue lasting 5 s was played and the sliding door between chambers B and C was opened by the experimenter. After that, the animal had access to chamber C, where it could find 5 sunflower seeds. The trial was over at the 300 s mark. This was repeated twice a day for 9 days, amounting for 18 trials. On the first trial of the $10^{th}$ day (the $19^{th}$ trial), the sunflower seed was replaced with crushed (picked) ice. On the last trial of the $10^{th}$ day (the $20^{th}$ trial), the sunflower seeds were placed as in all other previous trials. The duration of trial 19 and 20 and the timestamp for cue presentation was the same as the previous 18 trials. For this set of experiments, 6 animals (animals #26 to #31) underwent the surgical procedure for viral vector injection and cannula placement. Since only animals #26 and #29 survived through the whole experiment regimen, only their data will be considered. Trials in which photometry data were acquired are highlighted in figure 10. All animals were housed individually for the duration of the experiments. Photometry and behavioral data were recorded and analyzed as previously.

## 6. BEHAVIORAL PROCEDURE: SOCIAL ISOLATION AND FOOD DEPRIVATION PARADIGMS

Because we could find a *ΔF/F* signal indicating dopaminergic activity upon social interaction and food presentation, we tested the extent to which the signal would be heightened if we increased the incentive salience of these stimuli.

In order to do such, we subjected the animals to a 24h social isolation period and then food deprived them for 12 hours. The apparatus used for these behavioral trials was the same used for the pro-social behavioral procedure. Only chambers B and C were used in this set of experiments. Rats did not have access to chamber A. Only

animals #26 and #29 underwent these sets of experiments. Animals #26 and #29 were being housed together for the duration of the food deprivation trials.

For the social isolation trials, the animal attached to the fiber photometry system was placed in the chamber B of the apparatus. After 120 s, the cagemate, which was inside in a small cage (30.5 cm x 20 cm x 12 cm) with a top wire mesh to allow interaction through sight, smell and hearing, was placed in the chamber C of the apparatus and the sliding door was opened, thus allowing the rat attached to the photometry system to explore chamber C (trial 01). The trial was ended after 300 s. After trial 01, the animals were housed separately for 24 hours. After the isolation period, the animals were tested in the same apparatus in three different paradigms: with an empty small cage (trial 02), with the cagemate inside the small cage (trial 03) and then were allowed to freely interact with one another (trial 04). The stimulus was always introduced at the 120 s timepoint. Due to role reversal, both animals underwent each trial twice: first with animal #26 tethered to the fiber photometry system and once more with animal #29 being recorded.

For the food deprivation trials, the animals were kept in food deprivation for 12 hours and underwent a simple reward conditioning paradigm with sunflower seeds in the other compartment (similar to previous trials). The animal was placed in chamber B for 120 s, at this timepoint a sound cue lasting 5 s was played and the sliding door giving access to chamber C was opened, where the animals could find 5 sunflower seeds (trial 01). Afterwards, the same trial was repeated, but the sunflower seeds at the 120 s mark were omitted and instead presented at the 240 s mark (trial 02).

## 7. FIXATION OF TISSUE AND IMMUNOHISTOCHEMISTRY

Rats were deeply anesthetized with isoflurane. Their thoracic cavities were opened and 0.1 mL of heparin was injected directly to their hearts. Immediately after, the animals were perfused with 200 mL of 0.9% saline followed by 200 mL of a freshly prepared fixative (paraformaldehyde 4%, pH = 7.4). Brains were removed and post-fixated overnight. Coronal slices (50 µm) were made in a vibratome (Leica), washed with PBS (pH = 7.4) and permeabilized with PBS/ Triton 0.3% for 30 minutes. Slices

were then blocked with donkey serum (DS) (PBS/ Triton 0.3%/ DS 10%) and incubated with mouse anti-TH (1:500, MAB318 | Sigma-Aldrich) and chicken anti-GFP (1:500, A10262 | ThermoFischer) (PBS/ Triton 0.3%/ DS 5%/ 1:500 anti-TH/ 1:500 anti-GFP) overnight at 4ºC. Sections were washed with PBS/Triton 0.3% and incubated with secondary fluorescent Alexa antibodies (1:1000 ABCAM | Donkey Anti-Mouse IgG Alexa Fluor 488 | ab150105; and 1:1000 ABCAM | Donkey Anti-Chicken IgY Alexa Fluor 568 | ab175712) and stained with DAPI (1:10000). Sections were then mounted, coverslipped, and visualized through an Olympus Confocal microscope at the Centro de Microscopia e Microanálise (CMM)-UFRGS. ImageJ/Fiji analysis program (NIH, USA) was utilized to count the number of TH-positive (DA neurons) and GFP-positive neurons manually.

## 8. STATISTICAL ANALYSES AND DATA PLOTTING

MATLAB (2018b) was utilized for the pre-processing of photometry data and GraphPad Prism 8.0 were used to analyze and plot the data. The Area Under the Curve (AUC) was calculated for every trial in which the neural activity was recorded using the 30s immediately before and the 30s immediately after a given stimulus was presented to the rat. This time window was arbitrarily chosen because the reward consumption would normally be over after 30s of introducing the stimulus. A baseline of Y=-2 was considered in all AUC calculations. The majority of the recordings never went below Y=-2, so this value was chosen because it could account for the majority of trials without disproportionally amplifying $\Delta F/F$ data that went above Y=0. The Calculations of statistical significance were performed only for the AUC data. Paired one-way ANOVA was used to determine if the groups significantly differed from one another. In case the one-way ANOVA result indicated a statistically significant difference, paired Tuckey's post-hoc test was used to determine which groups differed from which. A difference was considered statistically significant if $p<0.05$. All figures were edited using Adobe Illustrator CS6/CC. Stock illustrations from Mind the Graph (mindthegraph.com) were used and adapted by the author.

# CHAPTER II – RESULTS

Evaluating neuronal function of genetically specified cell types in deep brain structures was not reliably possible before the advent of the fiber optic photometry technology (CUI et al., 2014). Fiber optic photometry has allowed neuroscientists to record fluorescence signals as a function of $Ca^{2+}$ dynamic shifts in neuronal cells at any depth. In the first use of this technology, DA signals from the SNc into the DMS and DLS of transgenic TH-Cre mice lineages were recorded (CUI et al., 2013).

Here, the results of the experiments described in the Materials and Methods section, as well as their interpretation, will be presented.

## INFECTION OF DOPAMINERGIC CELLS OF THE VTA BY A COMBINATION OF VIRAL VECTORS AND GENERAL CONSIDERATIONS ABOUT THE SURGERY

First, we needed to determine a suitable titre for viral delivery at which the infection of $TH^+$ cells by our viral mix would be effective. In the first 07 animals (Animals #01 to #07), custom made viral vectors were utilized unsuccessfully: no animal showed signs of viral infection when analyzed under the microscope. From rat #08 onward, the commercial viral vectors specified in the methods were utilized. Through the combination of these viral vectors, we aimed to achieve a TH+ cell specific GCaMP expression, since the DNA encoding for the Cre enzyme was under the TH promoter,

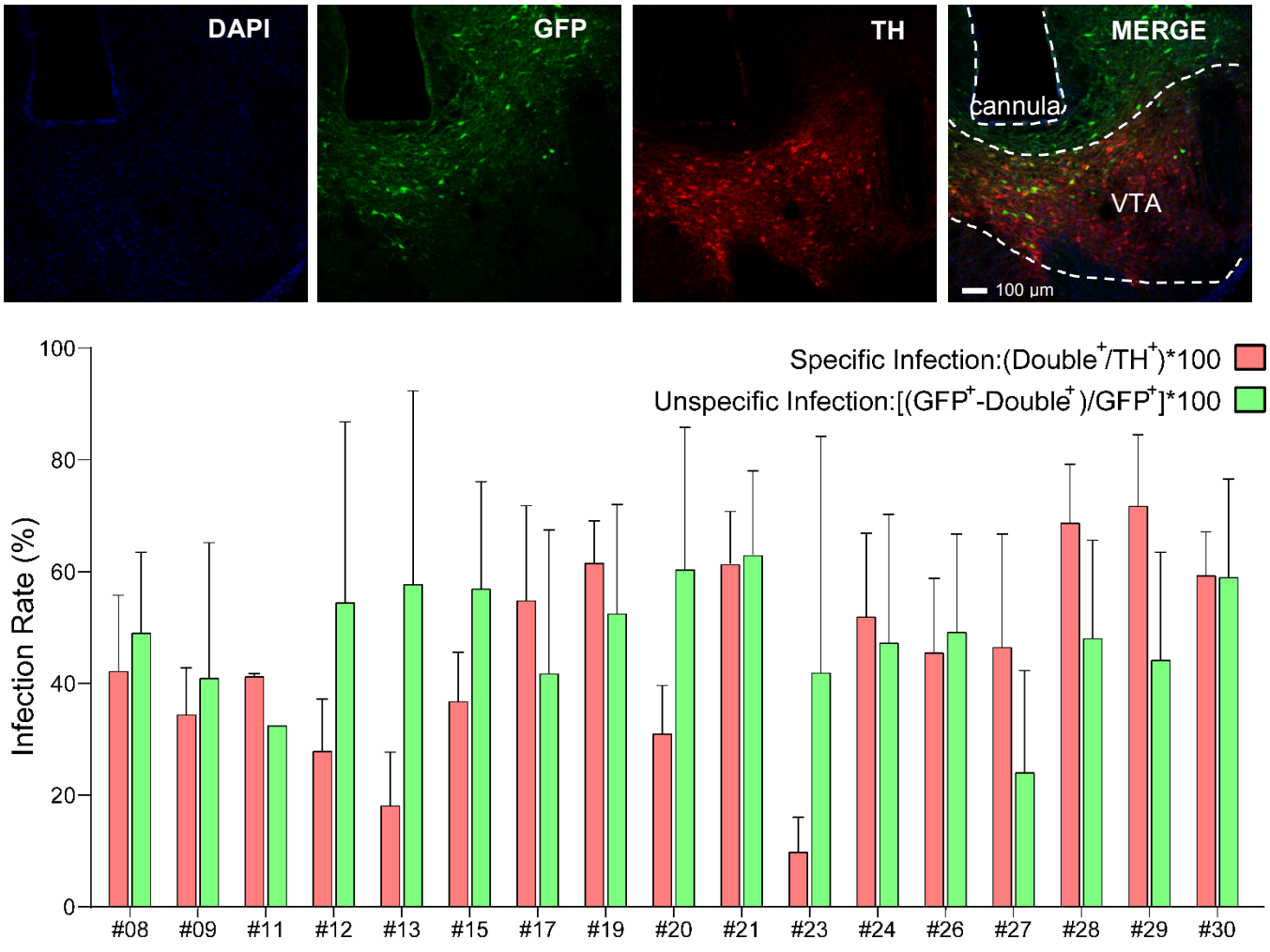


**FIGURE 7: Immunostaining and infection rates**
Top row: sample images (animal #26) taken in the confocal microscope. **(continues next page)**

and thus would theoretically have its expression restricted to cells that naturally express TH.

$TH^+$ and $TH^+$-$GFP^+$ ($Double^+$) were manually counted and the infection ratio was calculated as the percentage of $TH^+$ that were also $GFP^+$ ($Double^+$ / $TH^+$) under confocal microscopy (Figure 7). Our infection rate was varied, ranging from just above 10% (Animal #23) to around 80% (Animal #29). Average infection of all animals considered in the study was 44.96% (17.03% SD). Animals which the data are not shown is because of either unsuccessful infection or sample loss and were therefore excluded from this study. Detailed coordinates of viral injections as well as the dosages of the viral mix injected for each rat can be found in Table 1.

We hypothesize that the varying viral infection rate on TH+ cells were due to slight variations in surgery, which might happen due to the natural anatomic variation among subjects, and the presence of random DNA integration of the viral genes into the host cell genome (COLELLA; RONZITTI; MINGOZZI, 2018; GONÇALVES, 2005). In the majority of the body of literature on fiber photometry, the experiments use transgenic Cre mice that express the recombinase under specific promoters, whereas we used wildtype rats. This means that, for our infection to be successful, the same cell needed to be successfully infected by both vectors, which decreases the chance of successful expression of GCaMP6f in the target cells.

Another interesting finding was the apparent cell death seen in some of the sample tissues under the microscope (data not shown). It has been reported that AAV viral vectors can cause cell toxicity (BERNS; MUZYCZKA, 2017; GRIMM; BÜNING, 2017). Since we needed to use two different viral vectors, we put forth the argument that this could also have caused tissue damage, thus decreasing the effectiveness of the infection. We also found GFP+ cells that were not TH+ at an average rate of 48.5% (10.75% SD), meaning that the use of the combination of vectors could be causing

**FIGURE 7 (continues from previous page): Immunostaining and infection rates**
Bottom row: infection rates of all animals in which surgery was performed. Green bars indicate the rate of specific infection (calculated as the percentage of $Double^+$ ($TH^+$-$GFP^+$) that were also $TH^+$: $Double^+$/$TH^+$). Red bars indicate the rate of unspecific infection (calculated as the percentage of $Double^+$ that were not $TH^+$: ($GFP^+$- $Double^+$)/$GFP^+$). Animals not shown here were excluded from the study.

unspecific infection in non-dopaminergic cells. It is also possible that these cells do express TH at very low levels (not detected by immunostaining), but sufficient to transcribe the Cre recombinase and the floxed GCaMP6f gene. Moreover, VTA-DA cells that express TH mRNA but not the enzyme have already been described (MORALES; MARGOLIS, 2017); which could also help explain our relatively high rate of unspecific expression. We speculate that this unspecific infection did not caused much interference in our results, since the behavioral paradigms used were meant to highlight expected dopamine activity in the VTA and the signals we acquired match those expected from VTA dopaminergic cells. However, the nature of these TH-/GFP+ cells remains to be investigated.

The titre of viral vectors we utilized throughout the study remained standard: a total of 500 nl (0.5 µl) of the viral mix in a 1:1 ratio (250 nl of the TH-Cre virus - AAV9.rTH.PI.Cre.SV40 - at a titre of $6.98x10^{13}$ + 250 nl of the Cre dependent GCaMP6f virus - AAV1.CAG-Flex-GCaMP6f - at a titre of $1.13x10^{13}$) (Table 1).

Considering animals #08 through #31, we had a total of 21 rats that underwent the surgical procedure with the commercial viral vector injection. Out of those, most (18) survived the post-surgical recovery period. Only animals #10, #15 and #31 had to be euthanized due to poor recuperation after surgery, which was defined as weight loss of >10% in the first 3 days after surgery. However, our major problem was the detachment of the helmet securing the fiber optic cannula. Animals #14, #15, #16, #17, #18, #19, #20, #22, #25, #27, #28 and #30 had to be euthanized due to helmet lost, amounting to a total of 12 out of 18 (66.6%) lost subjects. Although loss of the dental cement helmet is not uncommon in optogenetic and fiber photometry experiments involving mice, it is noteworthy to point that rats are significantly stronger than mice, which might explain our relatively high percentage of lost animals. It is also notable that out of the 12 animals that lost their helmet, 10 (83.3%) (animals #16 to #30) came from other experiments (pro-social behavior) and were considerably older at the time of surgery (10 to 12 months of age). This points to age as a possible important factor for long term survival post-surgery, but not for the infection success *per se*, as the infection rates of these older animals did not differ from the younger ones. Lastly, taking into account the

experiments depicted in Figure 11, we can notice that the majority of helmet losses happened in the first 8 days of experiment (70%). At this time point, we were performing photometry recordings every day in these animals (#16 to #25), meaning that they were being attached to the photometry system on a daily basis. We speculate that this constant attachment and detachment to the photometry system might have loosened the helmet from their skulls. The animals, at times, would also show signals of discomfort during the procedure of attaching/detaching of the cannula to the photometry system. Because of this discomfort, we did not performed fiber photometry on days 13 to 15 on the experiments depicted in Figure 11. For the same reason, we chose not to perform fiber photometry measurements in a daily basis in the next set of experiments. In the experiment depicted in Figure 12, only 2 (animals #28 and #30) out of the 5 (animals #26 to #31) surviving animals (animal #31 was euthanized due to poor recuperation after surgery) lost their helmets in the beginning of the experiments (40%). This represents a decrease of 30% in animal loss due to helmet detachment.

**TABLE 1: Information details on the animals**

| Animal | Weight (g) | Injection Coordinates (LL/ AP) (cm from bregma) | Sex | Total volume injected (µl) | Specific Infection Rate (%) | Unspecific Infection Rate (%) |
|---|---|---|---|---|---|---|
| **#08** | Lost data | Lost data | M | 0.5 | 42.5 | 49.03 |
| **#09** | 488 | 2.05/4.12 | M | 0.5 | 33.41 | 48.49 |
| **#11** | 302 | 6.78/6.06 | F | 0.5 | 41.66 | 32.70 |
| **#12** | 459 | 6.88/5.87 | M | 0.5 | 25.99 | 58.85 |
| **#13** | 472 | 6.81/5.30 | M | 0.5 | 15.72 | 53.08 |
| **#15** | 414 | 6.65/6.00 | M | 0.5 | 37.65 | 49.34 |
| **#17** | 580 | 7.04/5.79 | M | 0.5 | 58.94 | 38.56 |
| **#19** | 624 | 7.12/5.81 | M | 0.5 | 60.78 | 54.72 |
| **#20** | 607 | 6.79/5.79 | M | 0.5 | 31.91 | 66.06 |
| **#21** | 640 | 6.79/5.64 | M | 0.5 | 61.40 | 63.19 |
| **#23** | 545 | 7.00/5.81 | M | 0.5 | 10.81 | 32.78 |
| **#24** | 625 | 6.67/5.67 | M | 0.5 | 51.10 | 45.39 |
| **#26** | 312 | 9.93/5.51 | F | 0.5 | 45.69 | 49.12 |
| **#27** | 295 | 6.69/5.92 | F | 0.5 | 48.39 | 27.77 |
| **#28** | 358 | 6.88/6.37 | F | 0.5 | 68.77 | 49.26 |
| **#29** | 305 | 6.80/6.02 | F | 0.5 | 70.30 | 43.14 |
| **#30** | 350 | 6.68/6.07 | F | 0.5 | 59.24 | 63.01 |

All animals considered in this table have been subjected to surgery for viral mix injection. Their sex, weight at time of surgery is provided, as well as the stereotaxic coordinates for the injection site and probe placement, the total volume injected and the average specific and unspecific infection rate for each animal. All viral mix preparations followed a 1:1 ratio of the viral vectors utilized: AAV1.CAG-Flex-GCaMP6f at titer $1.13x10^{13}$ and AAV9.rTH.PI.Cre.SV40 at titer $6.98x10^{13}$.

## DETECTION OF DOPAMINERGIC SIGNALING IN SIMPLE REWARD AND IN PAVLOVIAN CONDITIONING PARADIGMS POINT TO THE FUNCTIONAL DIVERSITY OF MESOLIMBIC DOPAMINERGIC CELLS

As mentioned, we chose the dopaminergic VTA cells because of their known responses to certain behavioral paradigms involving reward and motivation (BROMBERG-MARTIN; MATSUMOTO; HIKOSAKA, 2010a; FIORILLO, 2013; FISCHBACH-WEISS; REESE; JANAK, 2018; SATOH et al., 2003; SCHULTZ, 2013; STEINBERG et al., 2013). It is well established that the mesolimbic dopamine system, amongst other functions, is responsible for coding the reward values of positive stimuli (FIORILLO, 2013; SCLAFANI; TOUZANI; BODNAR, 2011). In light of that, we chose a simple reward paradigm as our first behavioral experiment in order to test whether the viral infection and cannula placement had been successful. We presented the animals with a 30% sucrose solution as a reward to elicit activity in the dopaminergic neurons from VTA (GUNAYDIN et al., 2014). If the surgery was successful, we expected to see an increase of dopaminergic activity upon reward presentation.

Animals were attached to the fiber photometry system and put in an open field for 600 s for habituation and signal stabilization. The reward was presented at 720 s and the test lasted for 900 s (Figure 8, A). The signal was acquired and $F$, $F_0$ and $\Delta F$ signals were calculated in MATLAB (Figure 8, D). When comparing the two panels in Figure 8D, it becomes clear that the $\Delta F/F$ calculation allows for correction of movement artifacts. As a quantitative measure of effect, the area under the curve (AUC) was calculated in 15 s bins for the 30 s immediately before and after the stimulus presentation for each trial. Data from animal #11 is depicted in Figure 8 as an example of the analyses performed for this set of experiments (Figure 8, B-C).

The same analyses were made for every rat that underwent this behavioral trial (Figure 9). Animal #11 presented a statistically significant difference among the AUC values of the times considered ($p=0.0091$, paired one-way ANOVA) (Figure 9, I), whereas animals #08 and #09 did not (Figure 9, G-H). Paired Tuckey's post-hoc test

indicated a statistically significant difference in -30 to -15s vs. 0 to 15 s (p=0.0166), -30 to -15 vs. 15 to 30 s (p=0.0165), and -15 to 0 s vs. 0 to 15 s (p=0.013) for animal #11.

Animals #08, #09 and #11 presented a similar viral infection rate of around 40%, but only animal #11 presented a statistically significant difference between the AUC of the 30 s before and after the rewarding stimuli. Interestingly, animal #11 presented peaks of over 10% of activity upon stimuli presentation (Figure 9, F), whereas animals #08 and #09 both presented peaks of around 1% (Figure 9, D-E). This difference is probably due to the anatomical differences regarding the fiber optic cannula placement. In studies of fiber photometry that investigate DA signals in transgenic mice, a 1% signal increase has been found and interpreted as a positive response to reward (ELLWOOD et al., 2017). And although animals #08 and #09 did not present a statistically significant difference between the analyzed AUCs, it is relevant to point that studies utilizing fiber photometry not always present a statistical calculation (CUI et al., 2013; ELLWOOD et

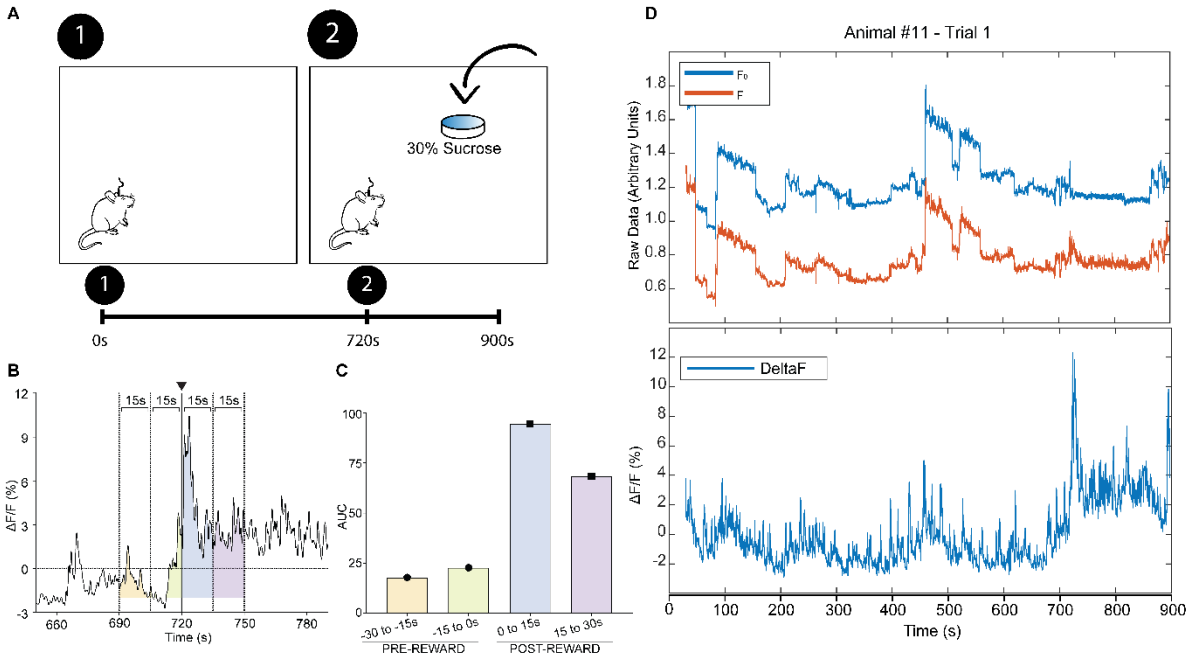


**FIGURE 8: Photometry recordings of a reward paradigm with 30% sucrose solution**
**(A)** The rats were placed in an open field and presented with a 30% sucrose solution as a reward at the 720 s mark. The trial duration was 900 s. **(B)** Sample recording of animal #11. Black triangle represents the time at which the sucrose solution was presented. Shaded areas represent the 15 s areas for which the AUC was calculated. **(C)** AUC of the highlighted areas in B. **(D)** Output analyses from MATLAB, where raw data (top panel) and *ΔF/F* (bottom panel) are depicted.

al., 2017), although some do calculate the AUC (BURNETT et al., 2016; YANG et al., 2018). Recently, a fiber photometry-based study using transgenic TH-Cre rats have also found variability in the *ΔF/F* signal amongst different subjects and considered a 1% variation in the *ΔF/F* signal as a positive marker for dopaminergic activity (MOHEBI et al., 2019). Taking this into account, we consider that animals #08 and #09 presented a positive response to the 30% sucrose solution, given the 1% increase in *ΔF/F*.

A caveat of using sucrose solution is that, since we used a camera positioned above

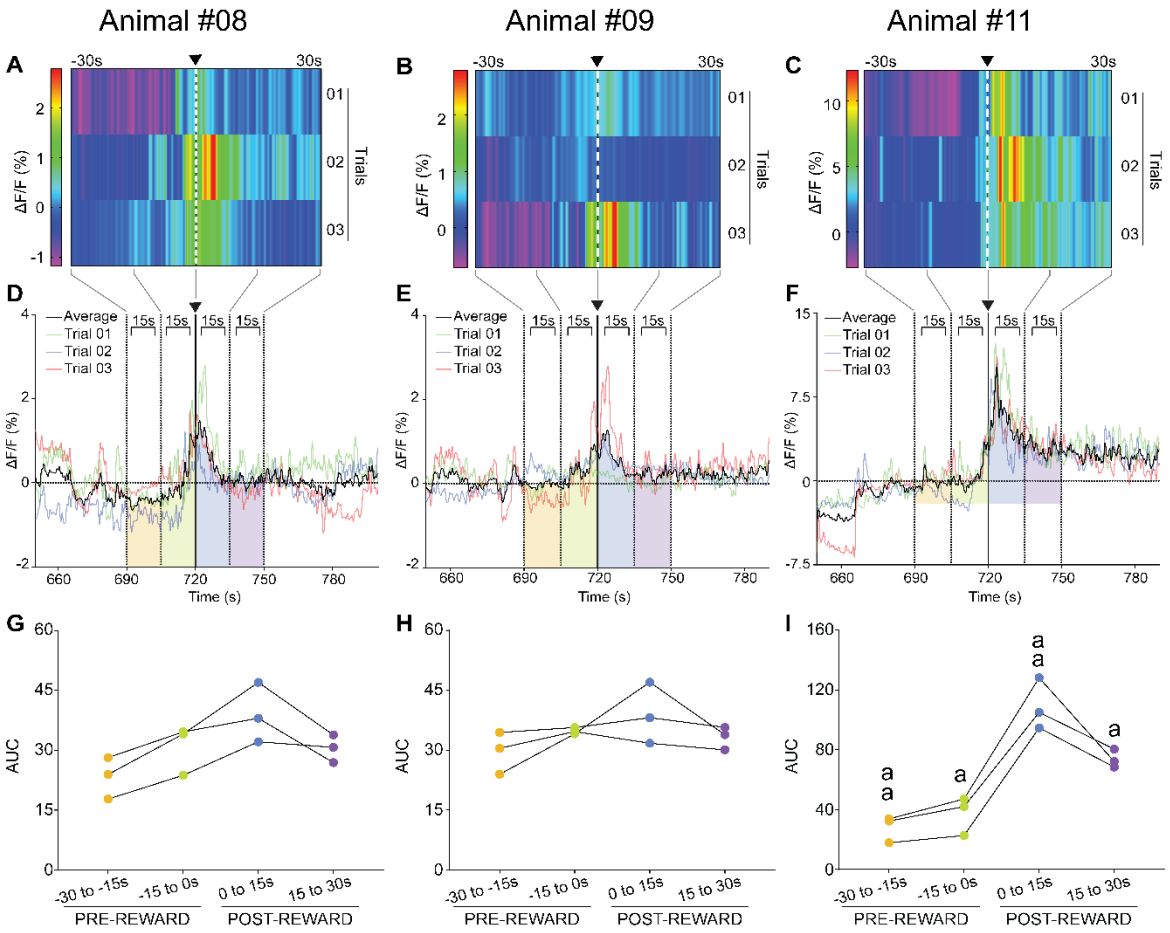


**FIGURE 9: Photometry recording of a reward paradigm with a 30% sucrose solution**
**(A-C)** Heatmap representation of the 1 minute around reward presentation (black triangle) of all 3 trials for each animal are depicted. **(D-F)** ΔF/F traces of every trial and the average signal are depicted for all 3 animals tested. Black triangle and black solid line represent the time at which the 30% sucrose solution was presented to the animals, dotted parallel lined represent the 15 s time windows. **(G-I)** The AUC of the 30s before reward presentation and the AUC of the 30s after the reward was presented, divided in 15 s bins, and are depicted for each animal. (I) p=0.0091, paired one-way ANOVA. Statistically significant differences were found in -30s to -15 s vs. 0 to 15 s (p= 0.0166), -30 to -15 s vs. 15 to 30 s (p=0.0165), and -15 to 0 s vs. 0 to 15 s (p=0.013). “a” = p<0.05.

the testing apparatus, we could not evaluate if the *ΔF/F* signal would peak when the animal consumed the sucrose as well as when the reward was presented to it, because we could not distinguish whether the animal was consuming the sucrose solution (licking) or only hovering its head above it. In order to circumvent that, we proceeded to present the animals with sunflower seeds, a treat present in the animal facility and used as an environmental enrichment element that the animals have a natural taste for and that we could have the precise time stamps of when they would eat. Animals were attached to the fiber photometry system for 300 s for habituation and signal stabilization. The reward was presented at 420 s and 540 s and the test was completed after 600 s (Figure 10, A). The signal was acquired as previously and the AUC was calculated as previously (Figure 10, B, E, H, K, N, Q). A representative sample recording is shown for every animal (Figure 10, D, G, J, M, P) and the signal of 1 minute around every stimulation for every trial is depicted for every animal that underwent this test (Figure 10, C, F, I, L, O).

Animal #11 presented a statistically significant difference among the analyzed AUCs ($p=0.0002$, paired one-way ANOVA). Tuckey's post-hoc test revealed a statistically significant difference between the following groups: -30 to 15 s vs. -15 to 0 s ($p<0.0001$), -30 to -15 s vs. 0 to 15 s ($p=0.0004$), and -30 to -15 s vs. 15 to 30 s ($p=0.0028$) (Figure 10, K). Interestingly, animal #08 also presented a statistically significant difference between the calculated AUCs ($p<0.0001$, paired one-way ANOVA). Tuckey's post-hoc test revealed a statistically significant difference between the following groups: -30 to 15 s vs. -15 to 0 s ($p<0.03371$), -30 to -15 s vs. 0 to 15 s ($p<0.0001$), -30 to -15 s vs. 15 to 30 s ($p<0.0001$), -15 to 0 s vs. 0 to 15 s ($p<0.0001$), and -15 to 0 s vs. 15 to 30 s ($p=0.0024$) (Figure 10, E). We speculate that this discrepancy between the results of animal #08 is due to the reduced number of trials in the previous paradigm (03 trials then and 13 trials now), especially when considering the traces depicted in Figure 9, where a clear peak of activity is visible upon reward presentation (Figure 9, D). When analyzed individually, the other animals (#09, #12 and #13) did not present statistically significant difference (Figure 10, H, N, Q). However, when the normalized AUC of all trials is considered, there is a statistically significant difference among the time windows analyzed ($p<0.0001$, paired one-way ANOVA).

Tuckey's post-hoc test revealed a statistically significant difference between the following groups: -30 to 15 s vs. -15 to 0 s ($p=0.0001$), -30 to -15 s vs. 0 to 15 s ($p<0.0001$), -30 to -15 s vs. 15 to 30 s ($p=0.0053$), and -15 to 0 s vs. 0 to 15 s ($p=0.0193$) (Figure 10, B).

The increase in the *ΔF/F* in dopamine expressing cells suggests that animals #08 and #11 responded positively to the sunflower seeds. Animal #09 did not present an increase in *ΔF/F* in most (8 out of 10) trials (Figure 10, F). Interestingly, animal #09 never showed interest in the stimulus presented (the sunflower seeds), as it rarely ate any (data not shown). There is variability in naturally occurring behaviors amongst animals of the same species (CHAMPAGNE et al., 2001; FONTANINI; KATZ, 2008; RÉALE et al., 2007), which could explain the fact that animal #09 in particular did not show interest for the sunflower seeds while the others did. Considering this behavioral pattern, we interpret the absence of fluorescence activity to corroborate the fact that the animal did not show interest for the rewards provided. Animal #12 presented an increase in *ΔF/F* when eating the seeds presented to it, but presented no signal change when it did not eat them. Animal #12 did not always eat the seeds or ate them at a delayed time, especially in the earlier sessions. This eating pattern could be due to the novelty that the stimulus represented in earlier trials. Rats are known to be neophobic (MODLINSKA; STRYJEK; PISULA, 2015), which could explain the lack of statistical significance when comparing the AUC of all animal #12 trials. Animal #13, which presented the second lowest infection rate of all animals tested (15.72%), did not present any change in signal upon reward presentation, regardless of whether it would eat the seeds or the novelty of the stimulus.

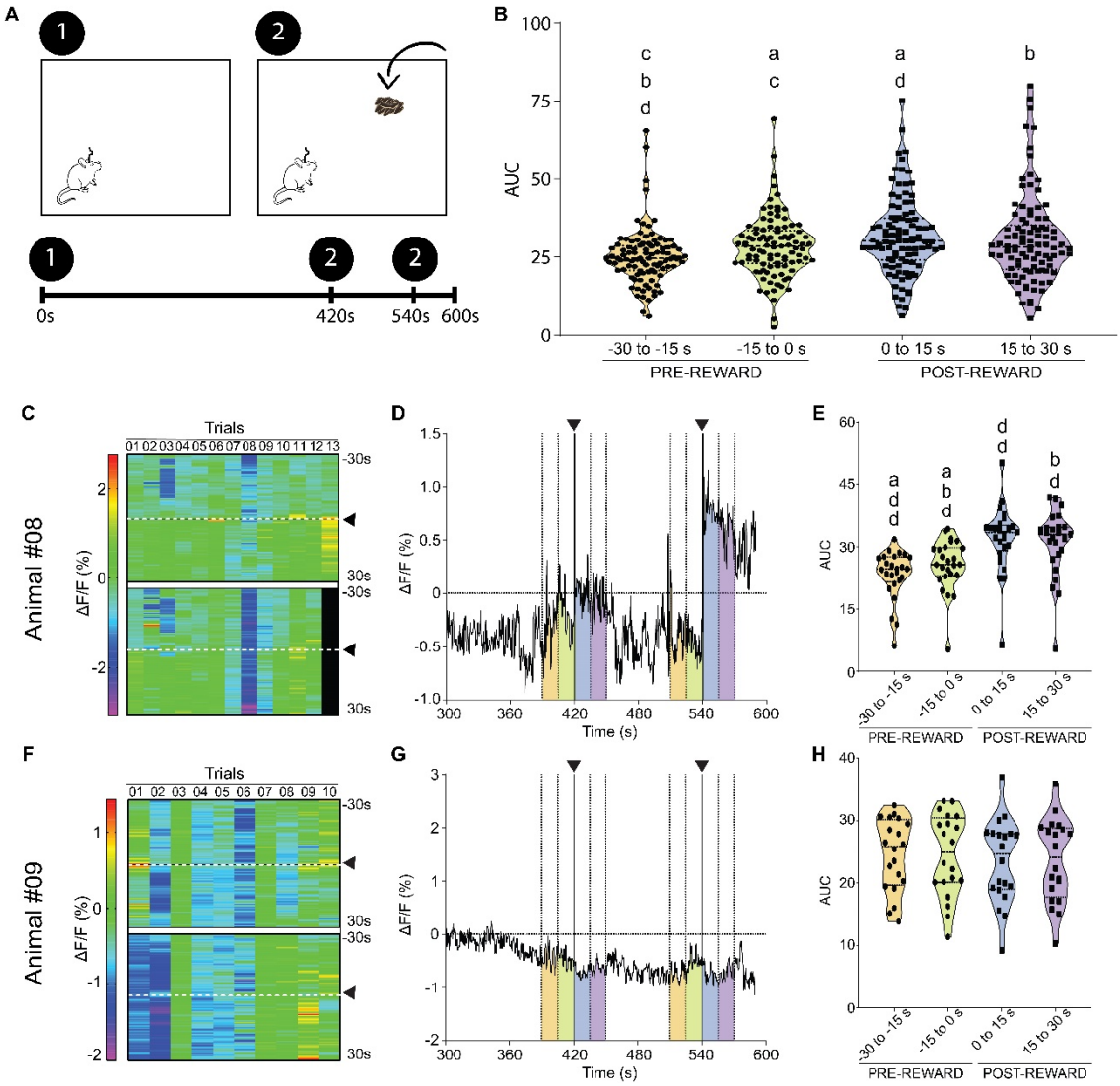


**FIGURE 10(a): Photometry recordings of a reward paradigm with sunflower seeds**

**(A)** The rats were placed in an open field and presented with sunflower seeds as a reward at the 420s and 540s time points. The trial duration was 600s. **(B)** The AUC for the 30s immediately before and after the reward presentation of every trial for every animal is depicted in 15 s bins. There is a statistically significant difference among the groups ($p<0.0001$, paired one-way ANOVA). Tucley's post-hoc test revealed significant differences between the following groups: -30 to 15 s vs. -15 to 0 s ($p=0.0001$), -30 to -15 s vs. 0 to 15 s ($p<0.0001$), -30 to -15 s vs. 15 to 30 s ($p=0.0053$), and -15 to 0 s vs. 0 to 15 s ($p=0.0193$). **(C)** Heatmap representation of 1 minute around reward presentation of every trial of animal #08. Black triangles mark the time points at which the reward was presented. **(D)** Sample trace of one animal #08 trial. Black triangles represent the time points at which reward was presented. Shaded areas represent the 15 s areas for which the AUC was calculated. **(E)** The AUC values of the shaded areas depicted in D for every animal #08 trial. Difference among the groups is statistically significant ($p<0.0001$, paired one-way ANOVA). Tuckey's post-hoc test revealed a statistically significant difference between the following groups: -30 to 15 s vs. -15 to 0 s ($p<0.03371$), -30 to -15 s vs. 0 to 15 s ($p<0.0001$), -30 to -15 s vs. 15 to 30 s ($p<0.0001$), -15 to 0 s vs. 0 to 15 s ($p<0.0001$), and -15 to 0 s vs. 15 to 30 s ($p=0.0024$). **(F)** Heatmap representation of 1 minute around reward presentation of every trial of animal #09. Black triangles mark the time points at which the reward was presented. **(G)** Sample trace of one animal #09 trial. Black triangles represent the time points at which reward was presented. Shaded areas represent the 15s areas for which the AUC was calculated. **(H)** The AUC values of the shaded areas depicted in G for every animal #09 trial. Difference between the groups is not statistically significant ($p=0.3009$, paired one-way ANOVA). "a" = $p<0.05$; "b" = $p>0.005$; "c" = $p<0.0005$; "d" = $p<0.0001$.

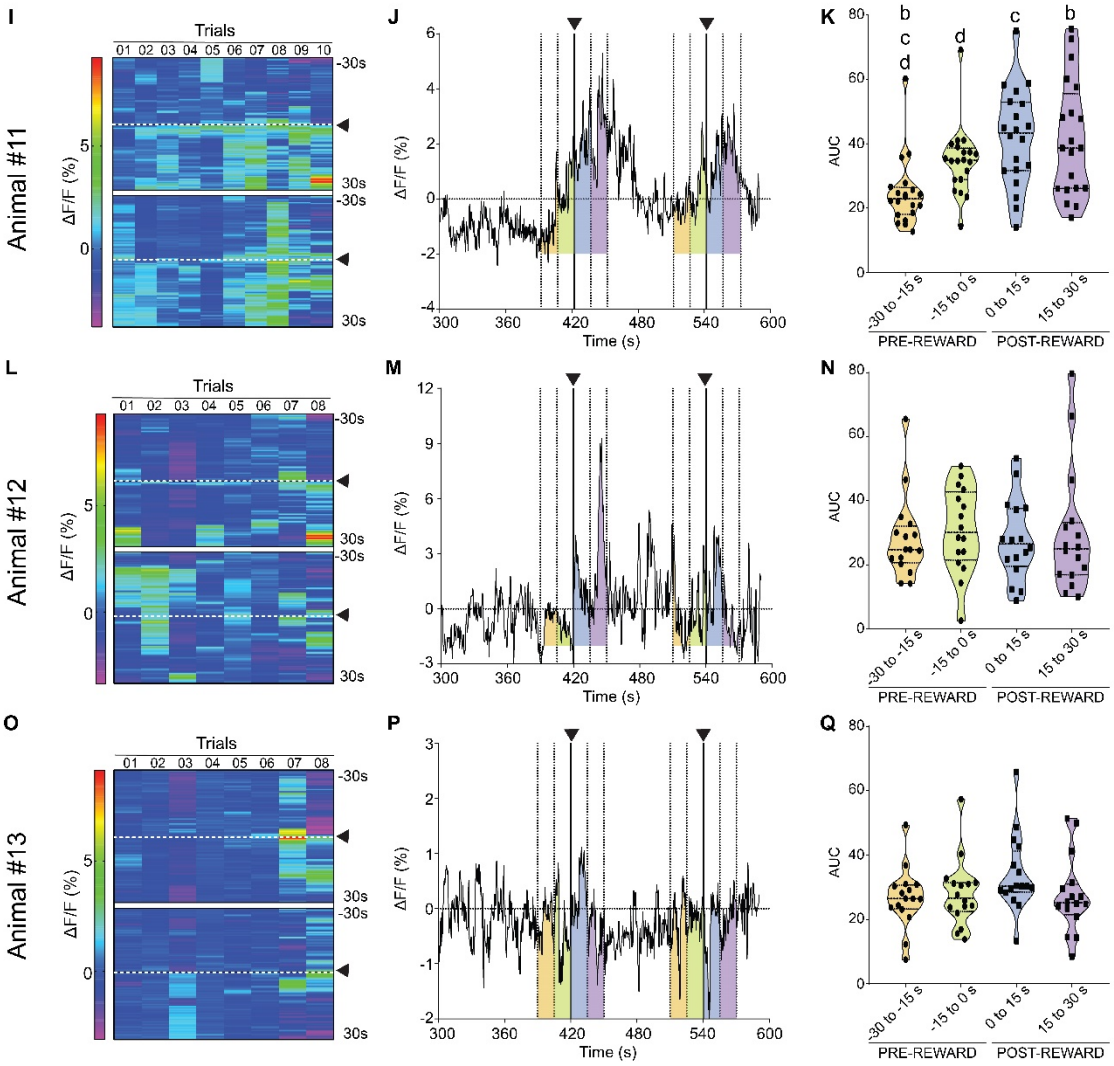


**FIGURE 10(b): Photometry recordings of a reward paradigm with sunflower seeds**

**(I)** Heatmap representation of 1 minute around reward presentation of every trial of animal #11. Black triangles mark the time points at which the reward was presented. **(J)** Sample trace of one animal #11 trial. Black triangles represent the time points at which reward was presented. Shaded areas represent the 15 s areas for which the AUC was calculated. **(K)** The AUC values of the shaded areas depicted in J for every animal #11 trial. Difference between the groups is statistically significant (p=0.0002, paired one-way ANOVA). Tuckey's post-hoc test revealed a statistically significant difference between the following groups: -30 to 15 s vs. -15 to 0 s (p<0.0001), -30 to -15 s vs. 0 to 15 s (p=0.0004), and -30 to -15 s vs. 15 to 30 s (p=0.0028). **(L)** Heatmap representation of 1 minute around reward presentation of every trial of animal #12. Black triangles mark the time points at which the reward was presented. **(M)** Sample trace of one animal #12 trial. Black triangles represent the time points at which reward was presented. Shaded areas represent the 30s areas for which the AUC was calculated. **(N)** The AUC values of the shaded areas depicted in M for every animal #12 trial. Difference between the groups is not statistically significant (p=0.8477, paired one-way ANOVA). **(O)** Heatmap representation of 1 minute around reward presentation of every trial of animal #13. Black triangles mark the time points at which the reward was presented. **(P)** Sample trace of one animal #13 trial. Black triangles represent the time points at which reward was presented. Shaded areas represent the 30s areas for which the AUC was calculated. **(Q)** The AUC values of the shaded areas depicted in P for every animal #08 trial. Difference between the groups is not statistically significant (p=0.11, paired one-way ANOVA). "a" = p<0.05; "b" = p>0.005; "c" = p<0.0005; "d" = p<0.0001.

When considering every trial and the individual pattern of each animal, we interpret these results depicted in Figure 9 to correctly indicate dopaminergic activity upon rewarding stimulus presentation in the majority (4 out of 5) of the animals tested. Due to the facts stated above, of the 5 animals that underwent the reward trials with sunflower seeds, we consider only data from animal #13 to be inconclusive.

A noticeable trend is the incremental increase in the AUC and F/F of the first three time windows considered (-30 to 15 s) and the decrease in the last time window (15 to 30 s). We speculate that this illustrates the anticipatory effect of receiving a reward, as dopamine neurons have been shown to respond to anticipation of rewards (BROMBERG-MARTIN; MATSUMOTO; HIKOSAKA, 2010b).

Although it is well established that dopaminergic VTA neurons encode the valence of positive stimuli, dopamine signaling has also been correlated with other functions related to motivation and reward-based learning (DAY et al., 2007; GORE; SODEN; ZWEIFEL, 2014; SCLAFANI; TOUZANI; BODNAR, 2011; YOUNG; MORAN; JOSEPH, 2005). For instance, studies using classical or Pavlovian conditioning paradigms have identified VTA-DA neurons that change their response over time: when pairing a rewarding unconditioned stimulus (US), such as food, to a conditioned stimulus (CS), a subpopulation of dopamine neurons will initially respond to both stimuli, but with time will eventually only respond to the CS. If the reward, at some point, becomes bigger than expected, these neurons become responsive again. This observation links dopamine function directly to the ability of outcome prediction through experience and learning (BROMBERG-MARTIN; MATSUMOTO; HIKOSAKA, 2010a; STEINBERG et al., 2013). Likewise, studies that take an instrumental or Skinner conditioning approach have linked dopaminergic transmission with incentive salience (the process through which a stimulus is conferred with motivational properties that make it more attractive), exertion of effort, decision making, effort-outcome cost balance (how much effort should be exerted into a given task based on its expected reward), risk assessment and probability-based outcome prediction (BEELER; FRAZIER; ZHUANG, 2012; BEIERHOLM et al., 2013; HOWE et al., 2013; SATOH et al., 2003; SCHULTZ, 2010; WESTBROOK; FRANK, 2018).

In order to further test the nature of the signal being acquired and to rule out the anticipatory effect, we next set out to test this signal in a Pavlovian conditioning paradigm in which the animal learns to associate a cue (CS) with presentation of a positive valence stimulus (reward) (US) in a new batch of animals (Animal #26 to #31) (Figure 11, A-B). With this approach, we expected that the animal would learn to associate the sound cue with the reward presentation. This protocol was repeated for 9 days, twice a day. On the 10$^{th}$ day, 19$^{th}$ trial, we replaced the sunflower seeds for picked (crushed) ice to evaluate how the signal would change when the reward was omitted and swapped for an aversive stimulus (Figure 11, A-B), as dopamine VTA cells have been reported to differently encode reward and frustration (DE JONG et al., 2019; MOHEBI et al., 2019). The 20$^{th}$ trial was done as all other previous trials and the experiment regimen was finalized afterwards. Since animals #26 and #29 were the only ones that remained alive at the end of the experiment (Figure 11, B) (all other animals had to be euthanized), only the data for these two animals are shown for each trial. Recorded data for every trial is shown for animals #26 (Figure 11, C-I) and #29 (Figure 11, K-P). Data for the first trial of animal #29 was lost.

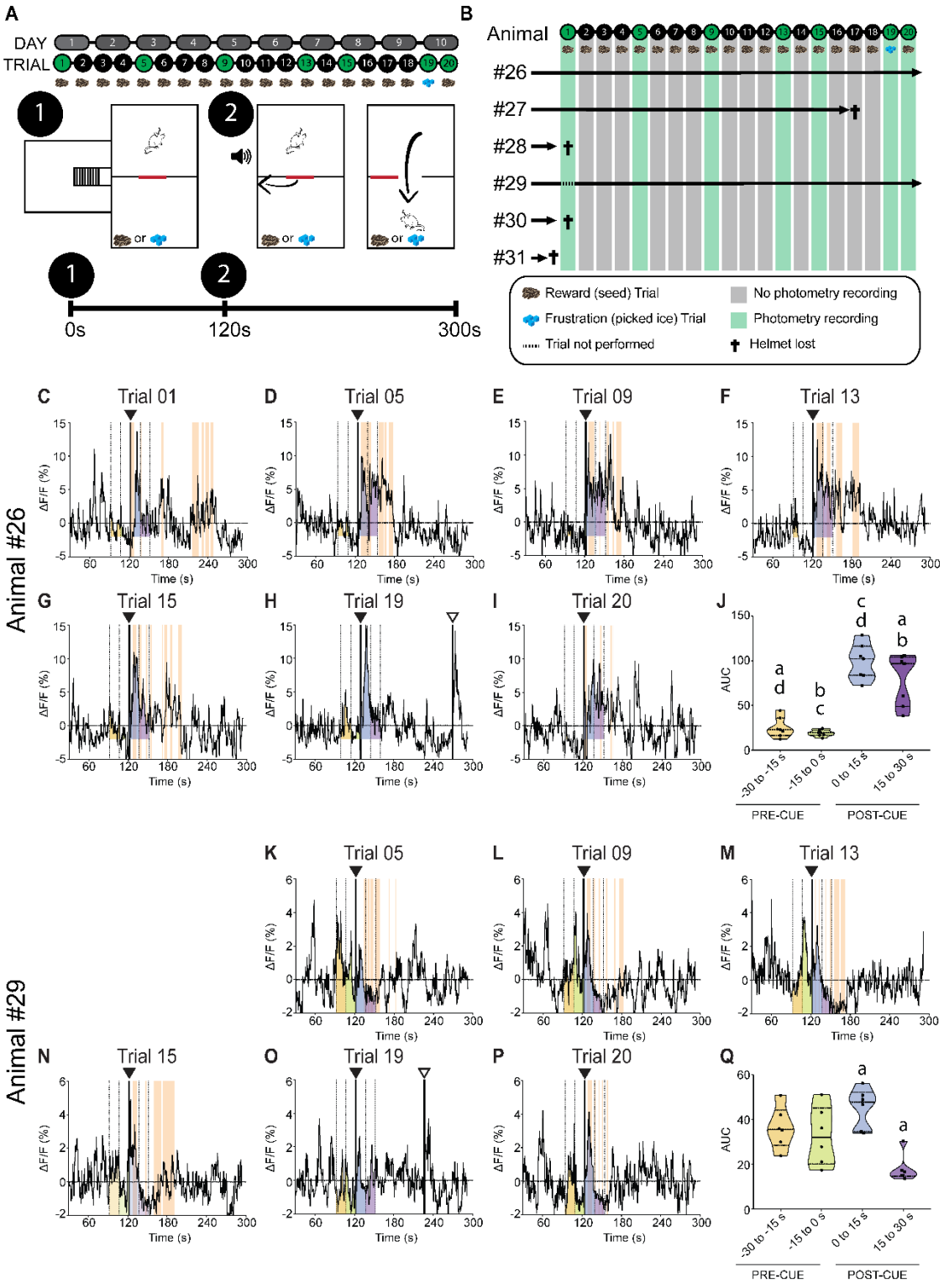


**FIGURE 11: Photometry recordings of a classical conditioning paradigm with sunflower seeds**
**(A)** The animal was placed in chamber B and after 120s a 5s sound cue was placed (CS) and the sliding door connecting chambers B and C was opened, allowing the animal to have access to 5 sunflower seeds (US) positioned in chamber C. **(B)** The experiment regimen was 10 days, two trials a day. Significant events are depicted in the legend. On the penultimate trial (named frustration trial), the sunflower seeds were replaced by picked ice. **(C-I)** The photometry recordings of every recorded trial of animal #26 is depicted. Black triangles represent the time point at which the sound cue was played. **(continues next page)**

In animal #26, a peak of activity can be observed when the sound cue was played as well as when the animal ate the sunflower seeds (Figure 11, C-G, I). In the frustration trial, however, an increase followed by a sharp decrease in the *ΔF/F* signal can be observed right after the sound cue (Figure 11, H, black triangle). Interestingly, a peak of activity can also be observed when the animal interacted with the picked ice, also followed by a sharp decrease (Figure 11, H, white triangle). Animal #29 appears to express a different pattern of activity. The *ΔF/F* peaked always when the sound cue was played, but sharply decreased when the animal ate the sunflower seeds (Figure 11, K-N, P). In the frustration trial, activity peaked when the cue was played (Figure 11, O, black triangle) and also when the animal interacted with the picked ice (Figure 11, O, white triangle). There was a statistically significant difference among the time windows analyzed for animal #26 ($p=0.003$, paired one-way ANOVA) and #29 ($p=0.0042$, paired one-way ANOVA). Tuckey's post-hoc test identified a difference for the following groups in animal #26: -30 to -15 s vs. 0 to 15 s ($p<0.0001$), -30 to -15 s vs. 15 to 30 s ($p=0.0334$), -15 to 0 s vs. 0 to 15 s ($p=0.0001$), and -15 to 0 s vs. 15 to 30 s ($p=0.0047$) (Figure 11, J). For animal #29, Tuckey's post-hoc test identified a statistically significant difference between two groups only: 0 to 15s vs. 15 to 30 s ($p=0.0175$) (Figure 11, Q).

**FIGURE 11 (continues from previous page): Photometry recordings of a classical conditioning paradigm with sunflower seeds**

White triangle represents the time point which the animal interacted with the picked ice. Orange shaded areas represent the time points in which the animal ate the sunflower seeds. Shaded areas underneath the trace represent the 15 s areas for which the AUC was calculated. **(J)** The AUC values of the shaded areas depicted in C-I for every animal #26 trial. Difference between the groups is statistically significant ($p=0.003$, paired one-way ANOVA) Tuckey's post-hoc test identified a difference for the following groups in animal: -30 to -15 s vs. 0 to 15 s ($p<0.0001$), -30 to -15 s vs. 15 to 30 s ($p=0.0334$), -15 to 0 s vs. 0 to 15 s ($p=0.0001$), and -15 to 0 s vs. 15 to 30 s ($p=0.0047$) . **(K-P)** The photometry recordings of every recorded trial of animal #29 is depicted. Black triangles represent the time point at which the sound cue was played. White triangle represents the time point which the animal interacted with the picked ice. Orange shaded areas represent the time points in which the animal ate the sunflower seeds. Shaded areas underneath the trace represent the 15 s areas for which the AUC was calculated. **(Q)** The AUC values of the shaded areas depicted in K-P for every animal #26 trial. Difference between the groups is statistically significant ($p=0.0042$, paired one-way ANOVA). Tuckey's post-hoc test identified a statistically significant difference between groups 0 to 15s vs. 15 to 30 s ($p=0.0175$). "a" = $p<0.05$, "b" = $p<0.005$, "c" = $p<0.0005$, "d" = $p<0.0001$

It is hypothesized that different mesolimbic dopaminergic cell subpopulations and circuits respond differently to different stimuli (BROMBERG-MARTIN; MATSUMOTO; HIKOSAKA, 2010a; DE JONG et al., 2019; GUNAYDIN et al., 2014; LAMMEL; LIM; MALENKA, 2014; LERNER et al., 2015; MENEGAS et al., 2018; MORALES; MARGOLIS, 2017; PALMITER, 2008; WISE, 2004). Some cells have been reported to respond to positive valence stimuli (FIORILLO, 2013), whereas other have been found to respond to negative valence stimuli (ESPINEL et al., 2018; NIEH et al., 2016), and others yet have been found to respond to salient stimuli (ROOT; ESTRIN; MORALES, 2018). In classical conditioning paradigms, positive-valence responding dopaminergic cells have been found to peak to both the US and the CS prior to learning the task, but, with increased repetition, they start to respond more strongly to the CS (DAY et al., 2007). Since in this study we aimed at general dopamine cells in the VTA, indistinctly of the neural circuitry they were a part of, it is unclear what subpopulation we were recording. We speculate that the dopaminergic cells recorded in animal #26 responded to both salience and positive valence, given the increased *ΔF/F* upon presentation of both CS and US on the reward trials and the peak *ΔF/F* upon CS and picked ice interaction on the frustration trial. However, we suspect to have only recorded the salience-responding dopaminergic VTA cells in animal #26, given the peak in *ΔF/F* recorded in every trial upon CS presentation and the increased *ΔF/F* when the animal interacted with the picked ice, a novel stimulus for the animals (it is important to point that the animals were used to the experimental set up when the experiments depicted in Figure 11 were performed, thus decreasing the novelty effect of the trial itself).

Next, we questioned whether increasing the incentive salience of the stimuli would also increase the *ΔF/F* signal. In order to do so, the animals were food deprived for 12 hours and submitted to a behavioral experiment similar to the ones done previously: the animals were put in chamber B of the apparatus for 120 s, time at which a sound cue was played and they were allowed access to chamber C, where they would find sunflower seeds (Figure 12, A, Trial 01). Afterwards, we tested whether the signal would present any alterations if the reward was omitted at the expected time and given at another time at which the animals were not used to. For that, we placed the animals in chamber B for 120 s, played the cue and allowed access to an empty chamber C.

The sunflower seeds were given to the animals after 240 s, instead of at 120 s, as they learnt to expect (Figure 12, A, Trial 02). In Trial 01, both animals responded as usual: animal #26 presented an increased *ΔF/F* upon cue and reward presentation (Figure 12, B) whereas animal #29 presented a peak in *ΔF/F* upon cue presentation (Figure 12, D). In the second trial, animal #26 seemed to present a depression in its usual signature *ΔF/F* upon reward omission, but presented a slightly higher *ΔF/F* elevation than in trial 01 when unexpectedly presented with reward (Figure 12, C). This is supported by other studies that attribute DA function to reward prediction, in which dopaminergic cells of

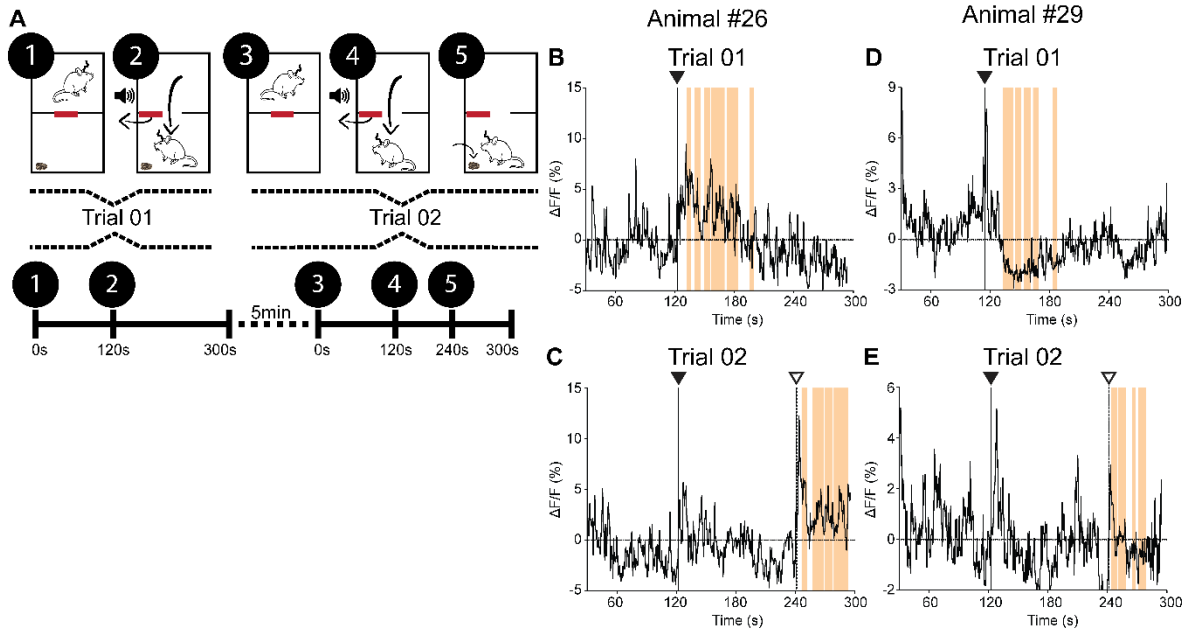


**FIGURE 12: Photometry recordings of social isolation and food deprivation paradigms**
**(A)** Trial 01: The animal was placed in chamber B and after 120s a 5s sound cue was played (CS) and the sliding door connecting chambers B and C was opened, allowing the animal to have access to 5 sunflower seeds (US) positioned in chamber C. Trial 02: The animal was placed in chamber B and after 120s a 5s sound cue was played (CS) and the sliding door connecting chambers B and C was opened, allowing the animal to have access to chamber C. The sunflower seeds (US) were presented at 240s. All trials lasted 300s. **(B)** Photometry recording of animal #26 trial 01. Black triangle represents the time at which the sound cue (CS) was played and the animal had access to the sunflower seeds (US). Orange shaded areas represent time stamps of when the animal ate the sunflower seeds. **(C)** Photometry recording of animal #26 trial 02. Black triangle represents the time at which the sound cue was played. White triangle represents the time at which the sunflower seeds were presented. Orange shaded areas represent time stamps of when the animal ate the sunflower seeds. **(D)** Photometry recording of animal #29 trial 01. Black triangle represents the time at which the sound cue (CS) was played and the animal had access to the sunflower seeds (US). Orange shaded areas represent time stamps of when the animal ate the sunflower seeds. **(E)** Photometry recording of animal #29 trial 02. Black triangle represents the time at which the sound cue was played. White triangle represents the time at which the sunflower seeds were presented. Orange shaded areas represent time stamps of when the animal ate the sunflower seeds.

conditioned animals present a decreased signal when the reward is as predicted, but increase firing upon receiving an unpredicted reward (BURKE; TOBLER, 2016; DAY et al., 2007; LANGDON et al., 2018; LAU; MONTEIRO; PATON, 2017; STEINBERG et al., 2013; SUGAM et al., 2012; TAKAHASHI et al., 2016; WATABE-UCHIDA; ESHEL; UCHIDA, 2017). Animal #29, on the other hand, showed the most significant increase in activity whenever a stimulus was presented (either CS or US), and not while consuming it (Figure 12, E). This finding supports our hypothesis that the subpopulation of cells being recorded in each animal was probably different. As mentioned, studies have found DA cells that only respond to salient stimuli, regardless of their valence (BARKER et al., 2016; SMITH; BERRIDGE; ALDRIDGE, 2011). We believe that to be the case with animal #26, whereas in animal #29 we might be recording DA cells more responsible for coding reward prediction error and positive valence stimuli.

Together, the results of these set of experiments point to the functional behavioral diversity amongst dopaminergic VTA neurons (LAMMEL; LIM; MALENKA, 2014; MORALES; MARGOLIS, 2017) and the caution needed when performing experiments using techniques that record neuronal bulk activity, as, for example, fiber photometry. A more in depth analyses can be done in the future by recording these neurons in a circuit-specific manner.

## DOPAMINERGIC VTA CELLS RESPOND TO SOCIAL INTERACTION

In our research group, efforts have been made to implement a new model for studying pro-social behaviors in which an observer animal can provide help for a demonstrator to leave an aversive situation (BARTAL; DECETY; MASON, 2011) or allow the demonstrator to have access to a rewarding stimulus (SATO et al., 2015). Rats are highly social animals and heightened dopaminergic activity upon social interaction has been recorded in these animals (GUNAYDIN et al., 2014). With that in mind, we set out to investigate whether we could detect dopaminergic activity in a pro-social paradigm we had previously standardized in our lab. A new batch of animals (animals #16 to #25) were used for this set of experiments. All animals have been previously trained in the task.

In this set of experiments, we aimed to analyze whether we could observe a peak of DA activity in the observer upon providing the demonstrator access to sunflower seeds (in chamber C) (Figure 13, A). As control experiments, we measured the signal response to receiving sunflower seeds (Figure 13, B) and whether the signal would be altered if chamber B was empty (Figure 13, C). In this control, we expect the latency to open the door to increase, as the observer animal would not be motivated to open the door if the demonstrator was absent, as previously found by our group (data not published) (Figure 13, E). This increase in the latency to open the door when no demonstrator was present points the socially motivated nature of such behavior. Since only animals #23 and #24 survived through the whole experiment regimen as a pair, only the data from these animals will be considered (Figure 10, D). Our hypothesis was that the observer animal would have an increase in dopaminergic activity upon presentation of reward to the demonstrator.

Animal #23 had a 10% of specific infection, the lowest among all tested animals, whereas animal #24 had an average infection rate of 51.1%. Both animals had inconclusive responses in the pro-social trials and the empty control, but seemed to have an increase in $\Delta F/F$ on the seed control trials. When these experiments were taking place, the animals were being housed individually; whereas they were being

housed in pairs while performing the original set of experiments. Although this could be interfering in the data, these results were inconclusive due to the small number of animals for which data were considered for analyses. However, one interesting finding was a slight increase in the *ΔF/F* when the demonstrator was placed in the apparatus (Figure 12, F, H, G and L, black triangle).

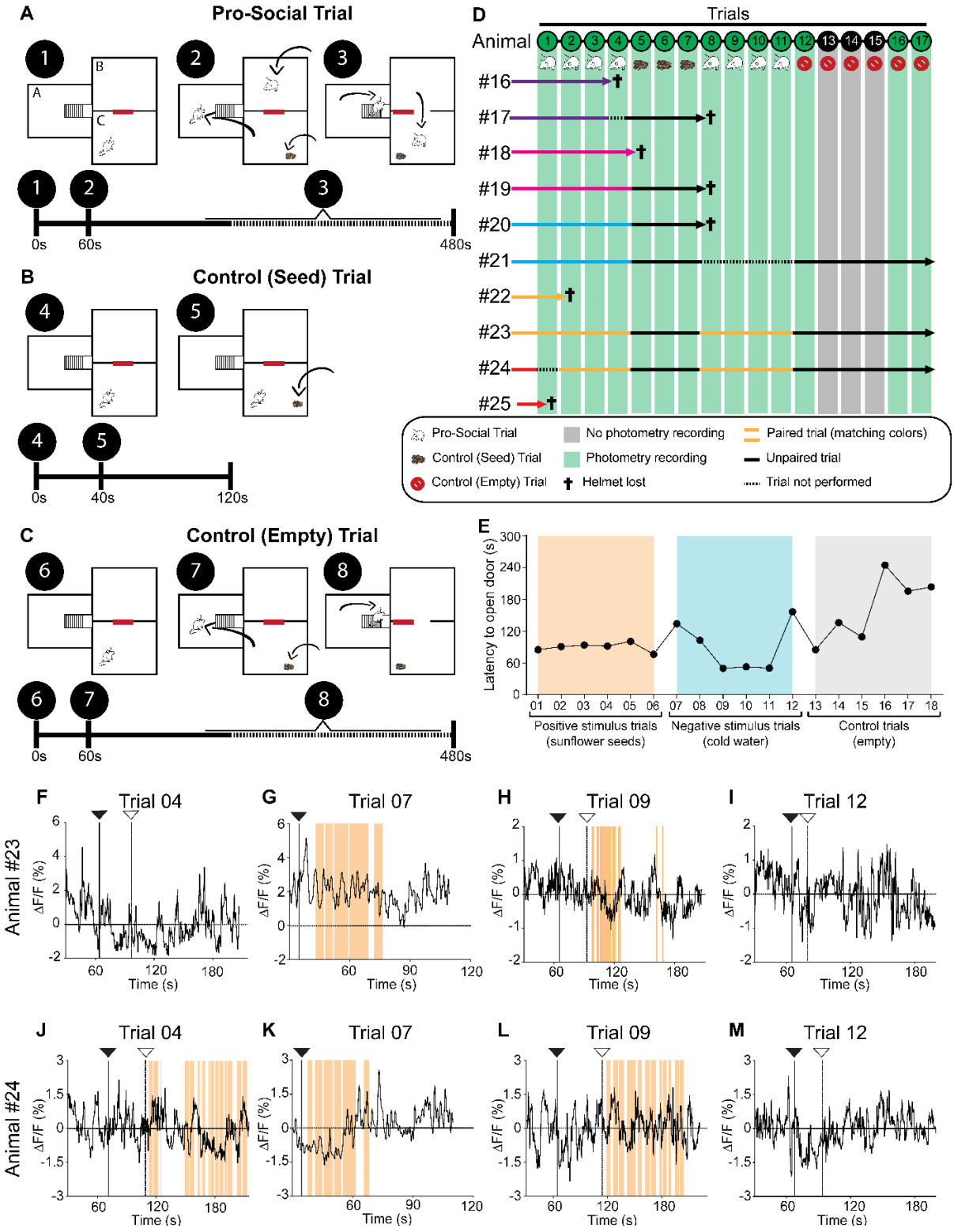


**FIGURE 13: Photometry recordings of a pro-social paradigm**

**(A)** Observer rat was placed in chamber C for 60s. At the 60s mark, the observer animal was placed in chamber A, the demonstrator animal was introduced in chamber B and 5 sunflower seeds were put in chamber C. The observer animal could climb a platform in chamber A in order to open the door between chambers B and C, thus allowing access to the sunflower seeds for the demonstrator animal. The trial was over 120s after the door was opened; the maximum trial duration was 480s. **(B)** The animal was placed in chamber C and was **(continues next page)**

In order to further investigate this matter and as a couple of last control experiments, we proceeded to submit animals from another batch (#26 and #29) to one additional behavioral test. Because we saw a peak in activity when the demonstrator was placed in the apparatus in the pro-social behavior paradigm (Figure 13, F, H, J and L, black triangle), we proceeded to perform a social interaction trial followed by a 24 hours isolation period. Animals #26 and #29 were being housed together when trial 01 (Figure 14, A) was performed: the cagemate was placed in the apparatus inside a small cage in which the free cagemate could interact trough smell, sight and hearing, but they were not allowed to freely touch each other. After trial 01, the animals were housed alone in separate cages for 24 hours. After the isolation period, the animals were tested in the same paradigm with an empty small cage as control (Figure 14, A, Trial 02), with the cagemate inside the small box (Figure 14, A, Trial 03) and then were allowed to freely interact with one another (Figure 14, A, Trial 04). Both animals underwent each trial twice: first with animal #26 tethered to the fiber photometry system and once more with animal #29 being recorded (Figure 14, B-I). The recording for each trial is depicted for animal #26 and #29 and times of social interaction bouts are highlighted in the orange shaded area of each graph. Although animal #26 has a stronger response, probably due to its higher infection rate, both animals show increased activity when interacting with their counterparts, either through the small cage wire mesh lid or when interacting freely. This corroborates findings of other studies that reported increased

**FIGURE 13 (continues from previous page): Photometry recordings of a pro-social paradigm**

given 5 sunflower seeds after 40s; the trial lasted 120s. (C)Same as A, but no demonstrator rat was used. (D)The experiment regimen was 17 days, one trial a day. Significant events are depicted in the legend. (E)Unpublished data from a parallel project depicting the latency for the observer animal to open the door to the demonstrator animal. An increase in the latency time to open the door is seen when there is no demonstrator in the apparatus. (F-G)Sample trials from animal #23. In F, H and I, black triangles represent the time the demonstrator was placed and white triangles represent the time at which animal #23 (observer) opened the door. In G, black triangle represents time at which the sunflower seeds were presented to animal #23. (J-M)Sample trials from animal #24. In J, K and M, black triangles represent the time the demonstrator was placed and white triangles represent the time at which animal #24 (observer) opened the door. In L, black triangle represents time at which the sunflower seeds were presented to animal #24.

dopaminergic activity in social interaction when measured through fiber photometry (GUNAYDIN et al., 2014) and microdialysis (HOLLY; DEBOLD; MICZEK, 2015).

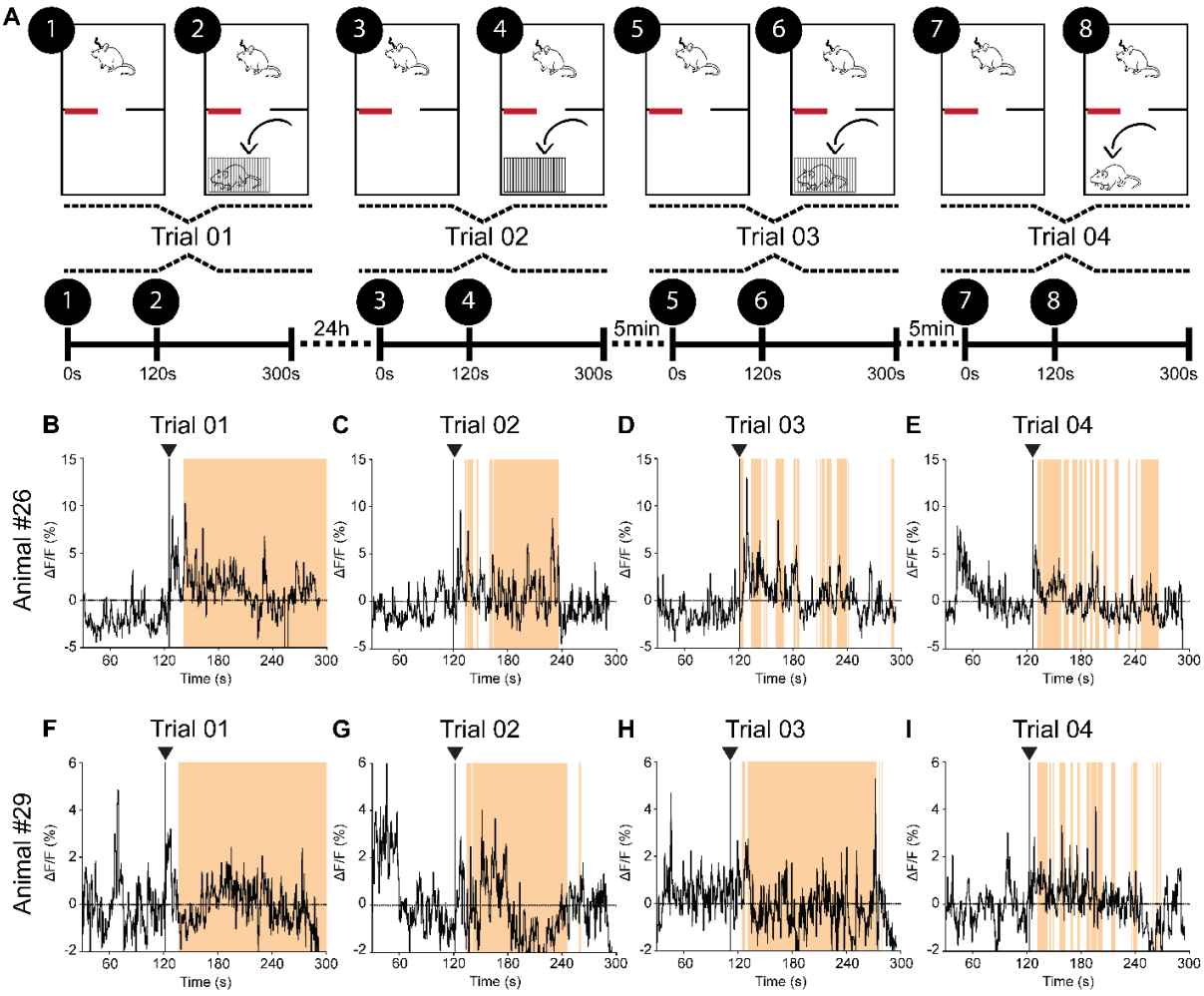


**FIGURE 14: Photometry recordings of social isolation and food deprivation paradigms**
**(A)** Trial 01: The animals were placed in chamber B and after 120s its cagemate was placed in chamber C inside a small box and the sliding door between chambers B and C was opened, allowing the animal in chamber B (attached to the photometry system) to interact with the animal inside the box through the wire mesh lid. After trial 01, the animals were housed in isolation for 24 hours. Trial 02: The animal was placed in chamber B and after 120s the sliding door between the cambers was opened. Trial 03: Same as trial 01. Trial 04: The animal was placed in chamber B and after 120s its cagemate was placed in chamber C and the sliding door between the two chambers were opened, thus allowing the animals to freely interact with one another. All trials lasted 300s. **(B-E)** The ΔF/F of every trial of animal #26 is shown. Orange shaded areas represent bouts of social interaction. Black triangles represent the time at which the partner was placed in chamber C. **(F-I)** The ΔF/F of every trial of animal #29 is shown. Orange shaded areas represent bouts of social interaction. Black triangles represent the time at which the partner was placed in chamber C.

# PART III

Here, the Discussion, Conclusions, Future Perspectives and References of this dissertation will be presented.

# DISCUSSION

## FIBER PHOTOMETRY AS A TOOL FOR PROBING DOPAMINERGIC NEURONAL SUBPOPULATIONS IN WILDTYPE RATS

As mentioned previously, fiber photometry allows for the recording of genetically specified cell populations in deep brain structures in freely behaving animals, something that was not possible before because of either depth impediments (in case of head mounted microscopy) or difficulty of precisely identifying the cells being recorded through the usage of electrodes (CUI et al., 2013, 2014; GUNAYDIN et al., 2014; WARDEN; CARDIN; DEISSEROTH, 2014). In this sense, fiber photometry emerges as a powerful tool for the analysis of neuronal dynamics and their correlation with behavioral expression. It is important to clarify, however, that this methodology also has its drawbacks.

One major caveat of using GECIs, such as GCaMP, is that they provide information derived from the magnitude and kinetics of calcium entry, binding and extrusion (O'SHEA et al., 2017). This means that membrane-localized transient events, such as channel dynamics or AP generation are amplified and transformed into a more prolonged biochemical change. An AP, for instance, takes 3-5 ms from initiation to completion, being over before the $[Ca^{2+}]_i$ change reached its peak (HELMCHEN; BORST; SAKMANN, 1997). As a result, GECIs are not well suited to report neurotransmitter receptor activation or AP firing with millisecond temporal precision and neither they are capable of providing data on membrane hyperpolarization or subthreshold voltage changes (GORE; SODEN; ZWEIFEL, 2014). Although an estimation of spike rates could be inferred from GECIs signal (LÜTCKE et al., 2013), this calculation is also difficult, as it depends on each individual cell GECI expression level, subcellular $Ca^{2+}$ localization and other variables. More recent permutations of GCaMP are addressing this issue, such as the new ultra bright jGCaMP7, which presents better kinetic properties than that of the GCaMP6 used in this work, although distinguishing individual spikes is not yet possible through the use of this GECI (DANA

et al., 2018). Other promising non-GCaMP GECIs with super-fast kinetics, that can better distinguish neuron spiking activity, are starting to be available for research use (PIATKEVICH et al., 2019), although their use is not yet widespread.

An important limitation of using fiber optic photometry is that, unlike head mounted microscopy or micro-endoscopy, it cannot distinguish individual cells being activated (LUO; CALLAWAY; SVOBODA, 2018a; WARDEN; CARDIN; DEISSEROTH, 2014). This means that any data acquired with this method needs to be interpreted as a result from neuronal aggregates, as it cannot provide results with resolution at the cellular level. Thus, when recording heterogeneous or asynchronous neuronal populations, *ΔF/F* might not be the ideal method.

Another important drawback is the tissue damage caused by the fiber optic probe. Although the diameter of the probes generally used are relatively small, they cannot be ignored, as the rate of tissue damage is a quadratic function of the radius of the object being inserted (CUI et al., 2014; GUO et al., 2015; SVOBODA; YASUDA, 2006). This is especially relevant when dealing with smaller animals, such as newborn rats and mice, which tissue can be detrimentally damaged by the insertion of a probe.

It is also important that the probe is well positioned and secured during the surgical procedure, as any dislocation could severely interfere with the data acquisition and bias the experiments. This is important to consider, given that fiber photometry allows for chronically recoding in the same animal over a time of weeks to months (CUI et al., 2014; WARDEN; CARDIN; DEISSEROTH, 2014), as it has also been done in the present study. An important risk also to be considered is the detachment of the dental cement helmet securing the probe, rendering the animal being experimented no longer useful for acquiring neuronal activity data.

It is also important to take into account the natural physiology of the area being recorded and its relation with behavioral expression. The VTA is a diverse and highly connected region (BEIER et al., 2015; LERNER et al., 2015). Not only dopamine, but also glutamate, GABA and combinatorial (which produce and release two or more transmitters, such as DA-Glutamate, GABA-DA and GABA-Glutamate) neurons have been identified in the VTA (MORALES; MARGOLIS, 2017). The functional specificity of

each of these neuronal subpopulations still remains largely unknown. Studies on the connectivity properties of these neurons has also yielded contrasting results. Results found in more recent literature suggests that the behavioral effect of VTA dopaminergic cells depend on the neural circuitry that they are a part of (DE JONG et al., 2019; MOHEBI et al., 2019; ROOT; ESTRIN; MORALES, 2018; YANG et al., 2018). As an example, studies have found that neurons in the lateral habenula (LHb) encode reward-prediction error, but in the opposite manner to the VTA. Accordingly, LHb optogenetic stimulation is enough to produce conditioned place aversion (LAMMEL et al., 2012) and other aversive behaviors (LECCA et al., 2017). Furthermore, stimulation of these LHb glutamatergic neurons seem to transiently inhibit DA-VTA neurons (STAMATAKIS et al., 2013). Some studies speculate that this effect is due to a di-synaptic connection in which aversive stimuli promotes LHb activation, which promotes activation of GABA-VTA local interneurons, ultimately leading to DA-VTA inhibition (DE JONG et al., 2019; TIAN; UCHIDA, 2015). Nonetheless, this fails to explain the observable increase in dopaminergic responses to aversive stimuli (DE JONG et al., 2019).

Another center correlated with dopamine functioning is the laterodorsal tegmentum nucleus (LTDg). The neurons in this region establish excitatory synapses onto $NAc_{shell}$-projecting DA-VTA neurons. Optogenetic stimulation of this mesolimbic-projecting LTDg subpopulation, contrary to LHb stimulation, produces conditioned place preference (LAMMEL et al., 2012; MORALES et al., 2016). However, MSNs in the NAc are not universally responsive only to positive-valence stimuli (ROOT; ESTRIN; MORALES, 2018). In both human (BALIKI et al., 2010; DELGADO; JOU; PHELPS, 2011; SEYMOUR et al., 2007) and non-human animal studies (ANSTROM; MICZEK; BUDYGIN, 2009; BUDYGIN et al., 2012; DE JONG et al., 2019; ESPINEL et al., 2018; LAMMEL et al., 2011; ROOT; ESTRIN; MORALES, 2018), activity in NAc has been correlated with both positive and negative valence stimuli. Recently, a study investigating the coding of reward-predicting error in the VTA dopaminergic cells of transgenic rats found a dissociation between reward expectation and reward-based learning in the mesolimbic dopaminergic system of these animals (MOHEBI et al., 2019), further pointing to the functional diversity within VTA dopaminergic neurons. We

hypothesize that this functional diversity within VTA might explain the contrasting results found in some of the animals used in the present study.

Even though these limitations need to be taken into account when performing experiments utilizing fiber optic photometry and interpreting its results, our data shows a clear activation of dopaminergic cells to reward, expectation and motivation related behaviors. Our results show an activity pattern that would be expected from DA mesolimbic systems in such behavioral paradigms and they are aligned with other studies using fiber optic photometry (CUI et al., 2013; DE JONG et al., 2019; ELLWOOD et al., 2017; GUNAYDIN et al., 2014). Therefore, our data supports wildtype Wistar rats as suitable models for the study of neuronal subpopulation dynamics through the method of fiber optic photometry.

# CONCLUSION

This works presents the results of our endeavor of implementing a new technology for measuring neuronal activity, the fiber optic photometry, for usage in our research group. The focus of this dissertation is methodological in nature, and we believe to have been successful in implementing this new technique and identified numerous potential roadblocks for its successful use. The patterns of activity found in the recording of the mesolimbic dopaminergic cells of the animals tested here fit with others found in literature.

The highest potential of fiber optic photometry as a tool for investigating neuronal functioning can be achieved when this and other techniques based on opto-neural interfaces (such as optogenetic) are used together with more traditional techniques, such as patch clamp in *ex vivo* preparations and *in vivo* extracellular voltage recordings, fast cycling voltammetry and microdialysis. New breakthroughs on the methods utilized to analyze morphology and connectivity within the nervous system, such as iDisco (RENIER et al., 2014), light sheet microscopy (POWER; HUISKEN, 2017) and CLARITY (JENSEN; BERG, 2017) can also be used in resonance with these previously mentioned techniques. These powerful tools, if properly used, can give new insights into long unanswered questions, shed new light on previously established dogmas, and open new venues in neuroscience research.

More than answering any particular theoretical question, this work opens doors for new research possibilities. For instance, using the technology implemented here, it is now possible to ask questions about specific neuronal circuitry and their relation to behavioral expression.

# FUTURE PERSPECTIVES

In attempting to better refine our methods, we tried to import three lineages of transgenic rats commonly used in other works when questioning about DA physiology: TH-Cre, D1R-Cre and D2R-Cre. After one and a half year of bureaucratic work, the animals were set to arrive in December 2018. However, due to last minute problems with the airline company, the shipment had to be cancelled and the rats needed to be euthanized by the sender. We believe that bringing transgenic rat lineages here would have allowed us to have better results, especially regarding the injection of the viral vectors, and would also have been a significant achievement for our local research community, as they would be available for any other research group. Bringing transgenic animals would also facilitate the study of DA physiology in newborn rats, an endeavor we tried to take (data not shown) but were unsuccessful in doing so.

Overall, however, we are optimistic with our results, as this is, to the best of our knowledge, the first time anyone has implemented fiber photometry for recording specific neuronal populations in wildtype rats. This allows us and our research community to tackle new and exciting research questions about distinct neuronal subpopulations and neuronal circuitry and their roles in shaping behavior.

# REFERENCES


AKERBOOM, J. et al. Optimization of a GCaMP Calcium Indicator for Neural Activity Imaging. **Journal of Neuroscience**, [s. l.], v. 32, n. 40, p. 13819–13840, 2012.

ANASTASSIADIS, Konstantinos et al. A practical summary of site-specific recombination, conditional mutagenesis, and tamoxifen induction of CreERT2. **Methods in Enzymology**, [s. l.], v. 477, n. C, p. 109–123, 2010.

ANDRÉ, Véronique M. et al. Dopamine modulation of excitatory currents in the striatum is dictated by the expression of D1 or D2 receptors and modified by endocannabinoids. **European Journal of Neuroscience**, [s. l.], v. 31, n. 1, p. 14–28, 2010.

ANSTROM, K. K.; MICZEK, K. A.; BUDYGIN, E. A. Increased phasic dopamine signaling in the mesolimbic pathway during social defeat in rats. **Neuroscience**, [s. l.], v. 161, n. 1, p. 3–12, 2009. Disponível em: <http://dx.doi.org/10.1016/j.neuroscience.2009.03.023>

BAKER, P. F.; HODGKIN, A. L.; RIDGWAY, E. B. Depolarization and calcium entry in squid giant axons. **The Journal of Physiology**, [s. l.], v. 218, n. 3, p. 709–755, 1971.

BALIKI, Marwan N. et al. Predicting Value of Pain and Analgesia: Nucleus Accumbens Response to Noxious Stimuli Changes in the Presence of Chronic Pain. **Neuron**, [s. l.], v. 66, n. 1, p. 149–160, 2010. Disponível em: <http://dx.doi.org/10.1016/j.neuron.2010.03.002>

BARKER, David J. et al. Multiplexed neurochemical signaling by neurons of the ventral tegmental area. **Journal of Chemical Neuroanatomy**, [s. l.], v. 73, p. 33–42, 2016. Disponível em: <http://dx.doi.org/10.1016/j.jchemneu.2015.12.016>

BARTAL, I. B. A.; DECETY, J.; MASON, P. Empathy and Pro-Social Behavior in Rats. **Science**, [s. l.], v. 334, n. 6061, p. 1427–1430, 2011. Disponível em: <http://www.sciencemag.org/cgi/doi/10.1126/science.1210789>

BEAULIEU, J. M.; GAINETDINOV, R. R. The Physiology, Signaling, and Pharmacology of Dopamine Receptors. **Pharmacological Reviews**, [s. l.], v. 63, n. 1, p. 182–217,

2011. Disponível em: <http://www.fedepapa.com/?page_id=419%5Cnfile:///D:/Descargas/preciocriollasinlavarb2012.xls>

BEAULIEU, Jean Martin; ESPINOZA, Stefano; GAINETDINOV, Raul R. Dopamine receptors - IUPHAR review 13. **British Journal of Pharmacology**, [s. l.], v. 172, n. 1, p. 1–23, 2015.

BEELER, Jeff A.; FRAZIER, Cristianne R. M.; ZHUANG, Xiaoxi. Putting desire on a budget: dopamine and energy expenditure, reconciling reward and resources. **Frontiers in Integrative Neuroscience**, [s. l.], v. 6, n. July, p. 1–22, 2012. Disponível em: <http://journal.frontiersin.org/article/10.3389/fnint.2012.00049/abstract>

BEIER, Kevin T. et al. Circuit Architecture of VTA Dopamine Neurons Revealed by Systematic Input-Output Mapping. **Cell**, [s. l.], v. 162, n. 3, p. 622–634, 2015. Disponível em: <http://dx.doi.org/10.1016/j.cell.2015.07.015>

BEIERHOLM, Ulrik et al. Dopamine modulates reward-related vigor. **Neuropsychopharmacology**, [s. l.], v. 38, n. 8, p. 1495–1503, 2013.

BERNS, Kenneth I.; MUZYCZKA, Nicholas. AAV: An Overview of Unanswered Questions. **Human Gene Therapy**, [s. l.], v. 28, n. 4, p. 308–313, 2017. Disponível em: <http://www.liebertpub.com/doi/10.1089/hum.2017.048>

BERRIDGE, Michael J.; LIPP, Peter; BOOTMAN, Martin D. The versatility and universality of calcium signalling. **Nature Reviews Molecular Cell Biology**, [s. l.], v. 1, n. 1, p. 11–21, 2000. Disponível em: <http://www.nature.com/articles/35036035>

BRANDA, Catherine S.; DYMECKI, Susan M. Talking about a revolution: The impact of site-specific recombinases on genetic analyses in mice. **Developmental Cell**, [s. l.], v. 6, n. 1, p. 7–28, 2004.

BREMER, F. Nouvelles recherches sur le mécanisme du sommeil. **C R Soc Biol**, [s. l.], v. 122, p. 460–464, 1936.

BROMBERG-MARTIN, Ethan S.; MATSUMOTO, Masayuki; HIKOSAKA, Okihide. Dopamine in Motivational Control: Rewarding, Aversive, and Alerting. **Neuron**, [s. l.], v.

68, n. 5, p. 815–834, 2010. a.

BROMBERG-MARTIN, Ethan S.; MATSUMOTO, Masayuki; HIKOSAKA, Okihide. Dopamine in Motivational Control: Rewarding, Aversive, and Alerting. **Neuron**, [s. l.], v. 68, n. 5, p. 815–834, 2010. b. Disponível em: <http://dx.doi.org/10.1016/j.neuron.2010.11.022>

BROUSSARD, Gerard J.; LIANG, Ruqiang; TIAN, Lin. Monitoring activity in neural circuits with genetically encoded indicators. **Frontiers in Molecular Neuroscience**, [s. l.], v. 7, n. December, 2014.

BUDYGIN, E. A. et al. Aversive stimulus differentially triggers subsecond dopamine release in reward regions. **Neuroscience**, [s. l.], v. 201, p. 331–337, 2012. Disponível em: <http://dx.doi.org/10.1016/j.neuroscience.2011.10.056>

BURKE, Christopher J.; TOBLER, Philippe N. Time, Not Size, Matters for Striatal Reward Predictions to Dopamine. **Neuron**, [s. l.], v. 91, n. 1, p. 8–11, 2016.

BURNETT, C. Joseph et al. Hunger-Driven Motivational State Competition. **Neuron**, [s. l.], v. 92, n. 1, p. 187–201, 2016.

CEPEDA, Carlos et al. Differential electrophysiological properties of dopamine D1 and D2 receptor-containing striatal medium-sized spiny neurons. **European Journal of Neuroscience**, [s. l.], v. 27, n. 3, p. 671–682, 2008.

CHAMPAGNE, F. et al. Naturally occurring variations in maternal behavior in the rat are associated with differences in estrogen-inducible central oxytocin receptors. **Proceedings of the National Academy of Sciences**, [s. l.], v. 98, n. 22, p. 12736–12741, 2001. Disponível em: <http://www.physiology.org/doi/10.1152/jn.90592.2008>

CHEN, Tsai Wen et al. Ultrasensitive fluorescent proteins for imaging neuronal activity. **Nature**, [s. l.], v. 499, n. 7458, p. 295–300, 2013.

CLAPHAM, David E. Calcium Signaling. **Cell**, [s. l.], v. 131, n. 6, p. 1047–1058, 2007. Disponível em: <https://linkinghub.elsevier.com/retrieve/pii/S0092867407015310>

COLELLA, Pasqualina; RONZITTI, Giuseppe; MINGOZZI, Federico. Emerging Issues in

AAV-Mediated In Vivo Gene Therapy. **Molecular Therapy - Methods and Clinical Development**, [s. l.], v. 8, n. March, p. 87–104, 2018. Disponível em: <https://doi.org/10.1016/j.omtm.2017.11.007>

CUI, Guohong et al. Concurrent activation of striatal direct and indirect pathways during action initiation. **Nature**, [s. l.], v. 494, n. 7436, p. 238–242, 2013. Disponível em: <http://dx.doi.org/10.1038/nature11846>

CUI, Guohong et al. Deep brain optical measurements of cell type-specific neural activity in behaving mice. **Nature Protocols**, [s. l.], v. 9, n. 6, p. 1213–1228, 2014.

CUMMINGS, Damian M. et al. Neuronal coupling via connexin36 contributes to spontaneous synaptic currents of striatal medium-sized spiny neurons. **Journal of Neuroscience Research**, [s. l.], v. 86, n. 10, p. 2147–2158, 2008.

DANA, Hod et al. High-performance GFP-based calcium indicators for imaging activity in neuronal populations and microcompartments. **bioRxiv**, [s. l.], p. 434589, 2018. Disponível em: <https://www.biorxiv.org/content/early/2018/10/03/434589>

DAY, Jeremy J. et al. Associative learning mediates dynamic shifts in dopamine signaling in the nucleus accumbens. **Nature Neuroscience**, [s. l.], v. 10, n. 8, p. 1020–1028, 2007.

DE JONG, Johannes W. et al. A Neural Circuit Mechanism for Encoding Aversive Stimuli in the Mesolimbic Dopamine System. **Neuron**, [s. l.], v. 101, n. 1, p. 133–151.e7, 2019. Disponível em: <https://doi.org/10.1016/j.neuron.2018.11.005>

DELGADO, Mauricio R.; JOU, Rita L.; PHELPS, Elizabeth A. Neural systems underlying aversive conditioning in humans with primary and secondary reinforcers. **Frontiers in Neuroscience**, [s. l.], v. 5, n. MAY, p. 1–10, 2011.

ELLWOOD, Ian T. et al. Tonic or Phasic Stimulation of Dopaminergic Projections to Prefrontal Cortex Causes Mice to Maintain or Deviate from Previously Learned Behavioral Strategies. **The Journal of Neuroscience**, [s. l.], v. 37, n. 35, p. 8315–8329, 2017. Disponível em: <http://www.jneurosci.org/lookup/doi/10.1523/JNEUROSCI.1221-17.2017>

ESPINEL, Isabella C. et al. Dopamine enhances signal-to-noise ratio in cortical-brainstem encoding of aversive stimuli. **Nature**, [s. l.], v. 563, n. 7731, p. 397–401, 2018. Disponível em: <http://dx.doi.org/10.1038/s41586-018-0682-1>

FIBIGER, H. C. Mechanisms: a Critical Review of the Catecholamine Theory. **Ann. Rev. Pharmacol. Toxicol**, [s. l.], v. 18, p. 37–56, 1978. Disponível em: <http://www.annualreviews.org/doi/pdf/10.1146/annurev.pa.18.040178.000345>

FIORILLO, C. D. Two Dimensions of Value: Dopamine Neurons Represent Reward But Not Aversiveness. **Science**, [s. l.], v. 341, n. 6145, p. 546–549, 2013. Disponível em: <http://www.ncbi.nlm.nih.gov/pubmed/23908236>

FISCHBACH-WEISS, Sarah; REESE, Rebecca M.; JANAK, Patricia H. Inhibiting Mesolimbic Dopamine Neurons Reduces the Initiation and Maintenance of Instrumental Responding. **Neuroscience**, [s. l.], v. 372, p. 306–315, 2018. Disponível em: <https://doi.org/10.1016/j.neuroscience.2017.12.003>

FONTANINI, Alfredo; KATZ, Donald B. Behavioral States, Network States, and Sensory Response Variability. **Journal of Neurophysiology**, [s. l.], v. 100, n. 3, p. 1160–1168, 2008. Disponível em: <http://www.physiology.org/doi/10.1152/jn.90592.2008>

GERFEN, Charles R.; SURMEIER, D. James. Modulation of Striatal Projection Systems by Dopamine. **Annual Review of Neuroscience**, [s. l.], v. 34, n. 1, p. 441–466, 2011. Disponível em: <http://www.annualreviews.org/doi/10.1146/annurev-neuro-061010-113641>

GONÇALVES, Manuel A. F. V. Adeno-associated virus: From defective virus to effective vector. **Virology Journal**, [s. l.], v. 2, p. 1–17, 2005.

GONG, S. et al. Targeting Cre Recombinase to Specific Neuron Populations with Bacterial Artificial Chromosome Constructs. **Journal of Neuroscience**, [s. l.], v. 27, n. 37, p. 9817–9823, 2007. Disponível em: <http://www.jneurosci.org/cgi/doi/10.1523/JNEUROSCI.2707-07.2007>

GORE, Bryan B.; SODEN, Marta E.; ZWEIFEL, Larry S. Visualization of plasticity in fear-evoked calcium signals in midbrain dopamine neurons. **Learning and Memory**, [s.

l.], v. 21, n. 11, p. 575–579, 2014.

GRIENBERGER, Christine; KONNERTH, Arthur. Imaging Calcium in Neurons. **Neuron**, [s. l.], v. 73, n. 5, p. 862–885, 2012. Disponível em: <http://dx.doi.org/10.1016/j.neuron.2012.02.011>

GRILLNER, Sten; ROBERTSON, Brita. The Basal Ganglia Over 500 Million Years. **Current Biology**, [s. l.], v. 26, n. 20, p. R1088–R1100, 2016. Disponível em: <http://dx.doi.org/10.1016/j.cub.2016.06.041>

GRIMM, Dirk; BÜNING, Hildegard. Small But Increasingly Mighty: Latest Advances in AAV Vector Research, Design, and Evolution. **Human Gene Therapy**, [s. l.], v. 28, n. 11, p. 1075–1086, 2017. Disponível em: <http://www.liebertpub.com/doi/10.1089/hum.2017.172>

GUNAYDIN, Lisa A. et al. Natural neural projection dynamics underlying social behavior. **Cell**, [s. l.], v. 157, n. 7, p. 1535–1551, 2014. Disponível em: <http://dx.doi.org/10.1016/j.cell.2014.05.017>

GUO, Qingchun et al. Multi-channel fiber photometry for population neuronal activity recording. **Biomedical Optics Express**, [s. l.], v. 6, n. 10, p. 3919, 2015. Disponível em: <https://www.osapublishing.org/abstract.cfm?URI=boe-6-10-3919>

HELMCHEN, Fritjof; BORST, J. Gerard G.; SAKMANN, Bert. Calcium dynamics associated with a single action potential in a CNS presynaptic terminal. **Biophysical Journal**, [s. l.], v. 72, n. 3, p. 1458–1471, 1997. Disponível em: <http://dx.doi.org/10.1016/S0006-3495(97)78792-7>

HOLLY, Elizabeth N.; DEBOLD, Joseph F.; MICZEK, Klaus A. Increased mesocorticolimbic dopamine during acute and repeated social defeat stress: Modulation by corticotropin releasing factor receptors in the ventral tegmental area. **Psychopharmacology**, [s. l.], v. 232, n. 24, p. 4469–4479, 2015.

HOWE, M. W.; DOMBECK, D. A. Rapid signalling in distinct dopaminergic axons during locomotion and reward. **Nature**, [s. l.], v. 535, n. 7613, p. 505–510, 2016. Disponível em: <http://dx.doi.org/10.1038/nature18942>

HOWE, Mark W. et al. Prolonged dopamine signalling in striatum signals proximity and value of distant rewards. **Nature**, [s. l.], v. 500, n. 7464, p. 575–579, 2013. Disponível em: <http://dx.doi.org/10.1038/nature12475>

HUDSPETH, A.J.; SCHWARTZ, JAMES; SIEGELBAUM, STEVEN; KANDEL, ERIC; JESSELL, Thomas; **Principles of Neural Science, Fifth Edition**. [s.l: s.n.].

IKEMOTO, Satoshi; YANG, Chen; TAN, Aaron. Basal ganglia circuit loops, dopamine and motivation: A review and enquiry. **Behavioural Brain Research**, [s. l.], v. 290, p. 17–31, 2015. Disponível em: <http://dx.doi.org/10.1016/j.bbr.2015.04.018>

JENSEN, Kristian H. Revele.; BERG, Rune W. Advances and perspectives in tissue clearing using CLARITY. **Journal of Chemical Neuroanatomy**, [s. l.], v. 86, p. 19–34, 2017. Disponível em: <https://doi.org/10.1016/j.jchemneu.2017.07.005>

KERKHOFS, M.; LAVIE, P. Frederic Bremer 1892–1982: a pioneer in sleep research. **Sleep Medicine reviews**, [s. l.], v. 4, n. 5, p. 505–514, 2000.

LAMMEL, Stephan et al. Projection-Specific Modulation of Dopamine Neuron Synapses by Aversive and Rewarding Stimuli. **Neuron**, [s. l.], v. 70, n. 5, p. 855–862, 2011. Disponível em: <http://dx.doi.org/10.1016/j.neuron.2011.03.025>

LAMMEL, Stephan et al. Input-specific control of reward and aversion in the ventral tegmental area. **Nature**, [s. l.], v. 491, n. 7423, p. 212–217, 2012. Disponível em: <http://dx.doi.org/10.1038/nature11527>

LAMMEL, Stephan; LIM, Byung Kook; MALENKA, Robert C. Reward and aversion in a heterogeneous midbrain dopamine system. **Neuropharmacology**, [s. l.], v. 76, n. PART B, p. 351–359, 2014. Disponível em: <http://dx.doi.org/10.1016/j.neuropharm.2013.03.019>

LANGDON, Angela J. et al. Model-based predictions for dopamine. **Current Opinion in Neurobiology**, [s. l.], v. 49, p. 1–7, 2018. Disponível em: <https://doi.org/10.1016/j.conb.2017.10.006>

LAU, Brian; MONTEIRO, Tiago; PATON, Joseph J. The many worlds hypothesis of dopamine prediction error: implications of a parallel circuit architecture in the basal

ganglia. **Current Opinion in Neurobiology**, [s. l.], v. 46, p. 241–247, 2017. Disponível em: <http://dx.doi.org/10.1016/j.conb.2017.08.015>

LECCA, Salvatore et al. Aversive stimuli drive hypothalamus-to-habenula excitation to promote escape behavior. **eLife**, [s. l.], v. 6, p. 1–16, 2017.

LERNER, Talia N. et al. Intact-Brain Analyses Reveal Distinct Information Carried by SNc Dopamine Subcircuits. **Cell**, [s. l.], v. 162, n. 3, p. 635–647, 2015. Disponível em: <http://dx.doi.org/10.1016/j.cell.2015.07.014>

LIN, Michael Z.; SCHNITZER, Mark J. Genetically encoded indicators of neuronal activity. **Nature Neuroscience**, [s. l.], v. 19, n. 9, p. 1142–1153, 2016.

LIU, Christine et al. A Neural Circuit Mechanism for Encoding Aversive Stimuli in the Mesolimbic Dopamine System. **Neuron**, [s. l.], v. 101, n. 1, p. 133–151.e7, 2018. Disponível em: <https://doi.org/10.1016/j.neuron.2018.11.005>

LUO, Liqun; CALLAWAY, Edward M.; SVOBODA, Karel. Genetic Dissection of Neural Circuits: A Decade of Progress. **Neuron**, [s. l.], v. 98, n. 2, p. 256–281, 2018. a.

LUO, Liqun; CALLAWAY, Edward M.; SVOBODA, Karel. Genetic Dissection of Neural Circuits: A Decade of Progress. **Neuron**, [s. l.], v. 98, n. 2, p. 256–281, 2018. b. Disponível em: <https://doi.org/10.1016/j.neuron.2018.03.040>

LÜTCKE, Henry et al. Inference of neuronal network spike dynamics and topology from calcium imaging data. **Frontiers in Neural Circuits**, [s. l.], v. 7, n. December, p. 1–20, 2013.

LYONS, Michelle R.; WEST, Anne E. Mechanisms of specificity in neuronal activity-regulated gene transcription. **Progress in Neurobiology**, [s. l.], v. 94, n. 3, p. 259–295, 2011. Disponível em: <http://dx.doi.org/10.1016/j.pneurobio.2011.05.003>

MALENKA, RC; NESTLER, EJ; HYMAN, SE. Widely Projecting Systems: Monoamines, Acetylcholine, and Orexin. In: **Molecular Neuropharmacology: A Foundation for Clinical Neuroscience**. [s.l: s.n.].

MARGOLIS, Elyssa B. et al. Reliability in the identification of midbrain dopamine

neurons. **PLoS ONE**, [s. l.], v. 5, n. 12, 2010.

MCLELLAN, Micheal A.; ROSENTHAL, Nadia A.; PINTO, Alexander R. Cre-loxP-Mediated Recombination: General Principles and Experimental Considerations. **Current protocols in mouse biology**, [s. l.], v. 7, n. 1, p. 1–12, 2017.

MENEGAS, William et al. Dopamine neurons projecting to the posterior striatum reinforce avoidance of theratening stimuli. **Nature neuroscience**, [s. l.], v. in press, n. October, 2018. Disponível em: <http://dx.doi.org/10.1038/s41593-018-0222-1>

MISHRA, Akanksha; SINGH, Sonu; SHUKLA, Shubha. Physiological and Functional Basis of Dopamine Receptors and Their Role in Neurogenesis: Possible Implication for Parkinson's disease. **Journal of Experimental Neuroscience**, [s. l.], v. 12, p. 117906951877982, 2018. Disponível em: <http://journals.sagepub.com/doi/10.1177/1179069518779829>

MODLINSKA, Klaudia; STRYJEK, Rafał; PISULA, Wojciech. Food neophobia in wild and laboratory rats (multi-strain comparison). **Behavioural Processes**, [s. l.], v. 113, p. 41–50, 2015. Disponível em: <http://dx.doi.org/10.1016/j.beproc.2014.12.005>

MOHEBI, Ali et al. Dissociable dopamine dynamics for learning and motivation. **Nature, Accepted**, [s. l.], 2019. Disponível em: <http://dx.doi.org/10.1038/s41586-019-1235-y>

MORALES, Marisela et al. Optogenetic excitation in the ventral tegmental area of glutamatergic or cholinergic inputs from the laterodorsal tegmental area drives reward. **European Journal of Neuroscience**, [s. l.], v. 45, n. 4, p. 559–571, 2016.

MORALES, Marisela; MARGOLIS, Elyssa B. Ventral tegmental area: Cellular heterogeneity, connectivity and behaviour. **Nature Reviews Neuroscience**, [s. l.], v. 18, n. 2, p. 73–85, 2017.

MOROZOV, Alexei. Conditional gene expression and targeting in neuroscience research. **Current Protocols in Neuroscience**, [s. l.], n. SUPPL. 44, p. 1–10, 2008.

NAGY, Andras. Cre recombinase: The universal reagent for genome tailoring. **Genesis**, [s. l.], v. 26, n. 2, p. 99–109, 2000.

NAKAI, J.; OHKURA, M.; IMOTO, K. A high signal-to-noise ca2+ probe composed of a single green fluorescent protein. **Nature Biotechnology**, [s. l.], v. 3, p. 137–141, 2001.

NEHER, Erwin; SAKABA, Takeshi. Multiple Roles of Calcium Ions in the Regulation of Neurotransmitter Release. **Neuron**, [s. l.], v. 59, n. 6, p. 861–872, 2008.

NESTLER, Eric J.; HEYMAN, Steven E.; MALENKA, Robert C. **Molecular Neuropharmacology A foundation for Clinical Neuroscience**. [s.l: s.n.].

NEVIAN, T.; SAKMANN, B. Spine Ca2+ Signaling in Spike-Timing-Dependent Plasticity. **Journal of Neuroscience**, [s. l.], v. 26, n. 43, p. 11001–11013, 2006. Disponível em: <http://www.jneurosci.org/cgi/doi/10.1523/JNEUROSCI.1749-06.2006>

NICOLA, Saleem M. The nucleus accumbens as part of a basal ganglia action selection circuit. **Psychopharmacology**, [s. l.], v. 191, n. 3, p. 521–550, 2007.

NIEH, Edward H. et al. Inhibitory Input from the Lateral Hypothalamus to the Ventral Tegmental Area Disinhibits Dopamine Neurons and Promotes Behavioral Activation. **Neuron**, [s. l.], v. 90, n. 6, p. 1286–1298, 2016. Disponível em: <http://dx.doi.org/10.1016/j.neuron.2016.04.035>

O'SHEA, Daniel J. et al. The need for calcium imaging in nonhuman primates: New motor neuroscience and brain-machine interfaces. **Experimental Neurology**, [s. l.], v. 287, p. 437–451, 2017. Disponível em: <http://dx.doi.org/10.1016/j.expneurol.2016.08.003>

OGAWA, Sachie K.; WATABE-UCHIDA, Mitsuko. Organization of dopamine and serotonin system: Anatomical and functional mapping of monosynaptic inputs using rabies virus. **Pharmacology Biochemistry and Behavior**, [s. l.], n. May, p. 1–14, 2017. Disponível em: <http://dx.doi.org/10.1016/j.pbb.2017.05.001>

PALMITER, Richard D. Dopamine signaling in the dorsal striatum is essential for motivated behaviors: Lessons from dopamine-deficient mice. **Annals of the New York Academy of Sciences**, [s. l.], v. 1129, p. 35–46, 2008.

PIATKEVICH, Kiryl D. et al. Population imaging of neural activity in awake behaving mice in multiple brain regions. [s. l.], 2019.

POULIN, Jean Francois et al. Defining midbrain dopaminergic neuron diversity by single-cell gene expression profiling. **Cell Reports**, [s. l.], v. 9, n. 3, p. 930–943, 2014. Disponível em: <http://dx.doi.org/10.1016/j.celrep.2014.10.008>

POWER, Rory M.; HUISKEN, Jan. A guide to light-sheet fluorescence microscopy for multiscale imaging. **Nature Methods**, [s. l.], v. 14, n. 4, p. 360–373, 2017.

PURVES, Dale et al. **Neuroscience**. 5th. ed. [s.l: s.n.].

RÉALE, Denis et al. Integrating animal temperament within ecology and evolution. **Biological Reviews**, [s. l.], v. 82, n. 2, p. 291–318, 2007.

RENIER, Nicolas et al. iDISCO: a simple, rapid method to immunolabel large tissue samples for volume imaging. **Cell**, [s. l.], v. 159, n. 4, p. 896–910, 2014. Disponível em: <http://www.ncbi.nlm.nih.gov/pubmed/25417164>

ROOT, David H.; ESTRIN, David J.; MORALES, Marisela. Aversion or Salience Signaling by Ventral Tegmental Area Glutamate Neurons. **iScience**, [s. l.], v. 2, p. 51–62, 2018. Disponível em: <http://linkinghub.elsevier.com/retrieve/pii/S2589004218300178>

SABATINI, Bernardo L.; OERTNER, Thomas G.; SVOBODA, Karel. The life cycle of Ca2+ ions in dendritic spines. **Neuron**, [s. l.], v. 33, n. 3, p. 439–452, 2002.

SALAMONE, John D. et al. Mesolimbic Dopamine and the Regulation of Motivated Behavior. In: **Brain Imaging in Behavioral Neuroscience**. [s.l: s.n.]. p. 231–257.

SALAMONE, John D. et al. Neurobiological basis of motivational deficits in psychopathology. **European Neuropsychopharmacology**, [s. l.], v. 25, n. 8, p. 1225–1238, 2015. b.

SALAMONE, John D. et al. The pharmacology of effort-related choice behavior: Dopamine, depression, and individual differences. **Behavioural Processes**, [s. l.], v. 127, p. 3–17, 2015. c. Disponível em: <http://dx.doi.org/10.1016/j.beproc.2016.02.008>

SALAMONE, John D.; CORREA, Mercè. The Mysterious Motivational Functions of Mesolimbic Dopamine. **Neuron**, [s. l.], v. 76, n. 3, p. 470–485, 2012.

SATO, Nobuya et al. Rats demonstrate helping behavior toward a soaked conspecific. **Animal Cognition**, [s. l.], v. 18, n. 5, p. 1039–1047, 2015. Disponível em: <http://dx.doi.org/10.1007/s10071-015-0872-2>

SATOH, T. et al. Correlated coding of motivation and outcome of decision by dopamine neurons. **The Journal of neuroscience : the official journal of the Society for Neuroscience**, [s. l.], v. 23, n. 30, p. 9913–9923, 2003.

SCHULTZ, Wolfram. Dopamine signals for reward value and risk: Basic and recent data. **Behavioral and Brain Functions**, [s. l.], v. 6, p. 1–9, 2010.

SCHULTZ, Wolfram. Updating dopamine reward signals. **Current Opinion in Neurobiology**, [s. l.], v. 23, n. 2, p. 229–238, 2013.

SCLAFANI, Anthony; TOUZANI, Khalid; BODNAR, Richard J. Dopamine and learned food preferences. **Physiology and Behavior**, [s. l.], v. 104, n. 1, p. 64–68, 2011. Disponível em: <http://dx.doi.org/10.1016/j.physbeh.2011.04.039>

SEYMOUR, B. et al. Differential Encoding of Losses and Gains in the Human Striatum. **Journal of Neuroscience**, [s. l.], v. 27, n. 18, p. 4826–4831, 2007.

SMITH, K. S.; BERRIDGE, K. C.; ALDRIDGE, J. W. Disentangling pleasure from incentive salience and learning signals in brain reward circuitry. **Proceedings of the National Academy of Sciences**, [s. l.], v. 108, n. 27, p. E255–E264, 2011. Disponível em: <http://www.pnas.org/cgi/doi/10.1073/pnas.1101920108>

SONG, Allisa J.; PALMITER, Richard D. Detecting and Avoiding Problems When Using the Cre–lox System. **Trends in Genetics**, [s. l.], v. 34, n. 5, p. 333–340, 2018. Disponível em: <http://dx.doi.org/10.1016/j.tig.2017.12.008>

STAMATAKIS, Alice M. et al. A Unique Population of Ventral Tegmental Area Neurons Inhibits the Lateral Habenula to Promote Reward. **Neuron**, [s. l.], v. 80, n. 4, p. 1039–1053, 2013. Disponível em: <http://dx.doi.org/10.1016/j.neuron.2013.08.023>

STAUFFER, William R. et al. Dopamine Neuron-Specific Optogenetic Stimulation in Rhesus Macaques. **Cell**, [s. l.], v. 166, n. 6, p. 1564–1571.e6, 2016. Disponível em: <http://dx.doi.org/10.1016/j.cell.2016.08.024>

STEINBERG, Elizabeth E. et al. A causal link between prediction errors, dopamine neurons and learning. **Nature Neuroscience**, [s. l.], v. 16, n. 7, p. 966–973, 2013. Disponível em: <http://dx.doi.org/10.1038/nn.3413>

SUGAM, Jonathan A. et al. Phasic nucleus accumbens dopamine encodes risk-based decision-making behavior. **Biological Psychiatry**, [s. l.], v. 71, n. 3, p. 199–205, 2012. Disponível em: <http://dx.doi.org/10.1016/j.biopsych.2011.09.029>

SURMEIER, D. J.; CARRILLO-REID, L.; BARGAS, J. Dopaminergic modulation of striatal neurons, circuits, and assemblies. **Neuroscience**, [s. l.], v. 198, p. 3–18, 2011. Disponível em: <http://dx.doi.org/10.1016/j.neuroscience.2011.08.051>

SVOBODA, Karel; YASUDA, Ryohei. Principles of Two-Photon Excitation Microscopy and Its Applications to Neuroscience. **Neuron**, [s. l.], v. 50, n. 6, p. 823–839, 2006.

SZCZYPKA, Mark S. et al. Dopamine production in the caudate putamen restores feeding in dopamine-deficient mice. **Neuron**, [s. l.], v. 30, n. 3, p. 819–828, 2001.

TAKAHASHI, Yuji K. et al. Temporal Specificity of Reward Prediction Errors Signaled by Putative Dopamine Neurons in Rat VTA Depends on Ventral Striatum. **Neuron**, [s. l.], v. 91, n. 1, p. 182–193, 2016. Disponível em: <http://dx.doi.org/10.1016/j.neuron.2016.05.015>

TIAN, Ju; UCHIDA, Naoshige. Habenula Lesions Reveal that Multiple Mechanisms Underlie Dopamine Prediction Errors. **Neuron**, [s. l.], v. 87, n. 6, p. 1304–1316, 2015. Disponível em: <http://dx.doi.org/10.1016/j.neuron.2015.08.028>

TINBERGEN, Nikolaas. **Animal Behavior**. [s.l: s.n.].

UNGLESS, Mark A.; MAGILL, Peter J.; BOLAM, J. Paul. Uniform Inhibition of Dopamine Neurons in the Ventral Tegmental Area by Aversive Stimuli. **Science**, [s. l.], v. 303, n. 5666, p. 2040–2042, 2004.

WARDEN, Melissa R.; CARDIN, Jessica A.; DEISSEROTH, Karl. Optical Neural Interfaces. **Annual Review of Biomedical Engineering**, [s. l.], v. 16, n. 1, p. 103–129, 2014. Disponível em: <http://www.annualreviews.org/doi/10.1146/annurev-bioeng-071813-104733>

WATABE-UCHIDA, Mitsuko et al. Whole-Brain Mapping of Direct Inputs to Midbrain Dopamine Neurons. **Neuron**, [s. l.], v. 74, n. 5, p. 858–873, 2012. Disponível em: <http://dx.doi.org/10.1016/j.neuron.2012.03.017>

WATABE-UCHIDA, Mitsuko; ESHEL, Neir; UCHIDA, Naoshige. Neural Circuitry of Reward Prediction Error. **Annual Review of Neuroscience**, [s. l.], v. 40, n. 1, p. 373–394, 2017.

WESTBROOK, Andrew; FRANK, Michael. Dopamine and proximity in motivation and cognitive control. **Current Opinion in Behavioral Sciences**, [s. l.], v. 22, p. 28–34, 2018. Disponível em: <https://doi.org/10.1016/j.cobeha.2017.12.011>

WISE, Roy A. Sensorimotor modulation and the variable action pattern (VAP): Toward a noncircular definition of drive and motivation. **Psychobiology**, [s. l.], v. 15, n. 1, p. 7–20, 1987.

WISE, Roy A. Dopamine, learning and motivation. **Nature Reviews Neuroscience**, [s. l.], v. 5, n. 6, p. 483–494, 2004.

YANG, Hongbin et al. Nucleus Accumbens Subnuclei Regulate Motivated Behavior via Direct Inhibition and Disinhibition of VTA Dopamine Subpopulations. **Neuron**, [s. l.], v. 97, n. 2, p. 434–449.e4, 2018. Disponível em: <https://doi.org/10.1016/j.neuron.2017.12.022>

YOUNG, Andrew M. J.; MORAN, Paula M.; JOSEPH, Michael H. The role of dopamine in conditioning and latent inhibition: What, when, where and how? **Neuroscience and Biobehavioral Reviews**, [s. l.], v. 29, n. 6, p. 963–976, 2005.

ZHANG, Jian et al. Conditional gene manipulation: Cre-ating a new biological era. **Journal of Zhejiang University SCIENCE B**, [s. l.], v. 13, n. 7, p. 511–524, 2012. Disponível em: <http://www.springerlink.com/index/10.1631/jzus.B1200042>

ZHOU, Qun Yong; PALMITER, Richard D. Dopamine-deficient mice are severely hypoactive, adipsic, and aphagic. **Cell**, [s. l.], v. 83, n. 7, p. 1197–1209, 1995.